Charge Control Strategy for Aircraft-Triggered Lightning Strike Risk Reduction

Charge Control Strategy for Aircraft-Triggered Lightning Strike Risk Reduction

Carmen Guerra-Garcia,* Ngoc Cuong Nguyen,† Jaime Peraire,‡ and Manuel Martinez-Sanchez§
Massachusetts Institute of Technology, Cambridge, Massachusetts 02139

DOI: 10.2514/1.J056406

We propose a charge control strategy to reduce the risk of an aircraft-triggered lightning strike that exploits the asymmetry between the positive and negative ends of the bidirectional leader development, which is the first phase of an aircraft-initiated lightning event. Because positive leaders are initiated and can propagate in lower fields than negative leaders, in general, a positive leader would occur first. During propagation of the positive leader, initiation of the negative leader is favored through the removal of positive charge from the aircraft. Based on this well-accepted bidirectional leader theory, we propose hindering the initiation of the positive leader by charging the aircraft to a negative level, selected to ensure that a negative leader will not form. Although not observed so far, a negative leader could be initiated first if the field enhancement at the negative end were much greater than at the positive end. In this situation, the biasing of the aircraft should be to positive levels. More generally, we propose that the optimum level of aircraft charging is that which makes both leaders equally unlikely. We present a theoretical study of the effectiveness of the strategy for an ellipsoidal fuselage as well as the geometry of a Falcon aircraft. The practical implementation, including the necessary sensors and actuators, is also discussed.

Nomenclature

a	=	major semi-axis of ellipsoid, m
b	=	minor semi-axis of ellipsoid, m
C	=	aircraft self-capacitance, F
c	=	focal distance of ellipsoid, m
d	=	diameter or distance, m
E	=	electric field amplitude, V/m
E_{cr}^{+}	=	breakdown threshold in positive polarity, constant field within positive streamer corona, V/m
E_{cr}^{-}	=	breakdown threshold in negative polarity, constant field within negative streamer corona, V/m
$E_{\max}$	=	maximum surface field, V/m
$E_{\min}$	=	minimum surface field, V/m
$E_{x,\infty}$	=	ambient electric field component in x direction, V/m
$E_{z,\infty}$	=	ambient electric field component in z direction, V/m
E_{∞}	=	ambient electric field amplitude, V/m
$(E_{\infty})_{\max}$	=	maximum ambient electric field amplitude that can be avoided using charge control, V/m
$\boldsymbol{E}$	=	electric field vector, V/m
$\boldsymbol{E}_n$	=	electric field on body (normal component), V/m
$\boldsymbol{E}_{(\cdot)}$	=	electric field vector due to $(\cdot)$, V/m
$\boldsymbol{E}_{\infty}$	=	ambient electric field vector, V/m
$\boldsymbol{e}$	=	nondimensional electric field vector
$\boldsymbol{e}_{(\cdot)}$	=	nondimensional electric field vector due to $(\cdot)$
f	=	fraction of energy that goes to gas heating
h	=	thermal enthalpy, J
h_η, h_ξ	=	shape factors
I	=	current, A
k	=	Boltzmann constant; 1.38×10^{-23} J/K
l	=	length, m
$\boldsymbol{M}$	=	nondimensional geometry dependent matrix
N	=	negative/positive breakdown threshold ratio
n	=	number density of gas, m^{-3}
n_0	=	initial number density of gas, m^{-3}
Q	=	charge, C
Q_{ac}	=	aircraft net charge, C
Q_{opt}	=	optimum net charge in terms of lightning avoidance, C
Q_{cr}^{+}	=	critical corona charge for positive leader formation, C
Q_{cr}^{-}	=	critical corona charge for negative leader formation, C
$\bar{Q}$	=	dimensionless aircraft net charge
q	=	ion charge, C
R	=	cylindrical radius, m
R_f	=	aircraft fuselage radius, m
r	=	plasma channel radius, m
r_0	=	initial plasma channel radius, m
S	=	surface, m^2
T	=	temperature, K
T_0	=	reference or initial gas temperature and time at first leader inception, K and s, respectively
T_{cr}	=	critical gas temperature for leader formation, K
t	=	time, s
U_{∞}	=	wind speed, m/s
$\boldsymbol{U}_{\infty}$	=	wind velocity vector, m/s
$\bar{U}$	=	wind parameter
$\boldsymbol{v}$	=	velocity field vector, m/s
x	=	coordinate orthogonal to axis of revolution of ellipsoid, m
x, y, z	=	aircraft axes, m
z	=	coordinate along axis of revolution of ellipsoid, m
α	=	geometry-dependent coefficient to evaluate maximum and minimum surface fields, $\mathrm{m}^{-1}\mathrm{F}^{-1}$
β	=	geometry-dependent coefficient to evaluate maximum and minimum surface fields
ε_0	=	permittivity of free space; 8.85×10^{-12} $\mathrm{A}^2 \cdot \mathrm{s}^4 \cdot \mathrm{kg}^{-1} \cdot \mathrm{m}^{-3}$
ϵ	=	small parameter
θ, φ	=	orientation of ambient field with respect to aircraft axis, rad
λ	=	aspect ratio of ellipsoid
μ_i	=	ion mobility, $\mathrm{m}^2\mathrm{s}^{-1}\mathrm{V}^{-1}$
ξ, η, φ	=	nondimensional prolate spheroidal coordinates

Received 19 June 2017; revision received 9 December 2017; accepted for publication 19 January 2018; published online 5 March 2018.

*Assistant Professor, Department of Aeronautics and Astronautics, 77 Massachusetts Avenue; previously Research Engineer, Boeing Research and Technology Europe, Avenida Sur del Aeropuerto de Barajas 38, Madrid, Spain, 28042; guerrac@mit.edu. Member AIAA.

†Research Scientist, Department of Aeronautics and Astronautics, 77 Massachusetts Avenue. Member AIAA.

‡Professor, Department of Aeronautics and Astronautics, 77 Massachusetts Avenue. Fellow AIAA.

§Professor Emeritus, Department of Aeronautics and Astronautics, 77 Massachusetts Avenue. Senior Member AIAA.

ξ_0 = shape factor of ellipsoid
Σ_c = corona surface, m^2
σ = surface charge, C/m^2
ϕ = electrostatic potential, V
ϕ_0 = electrostatic potential of body, V
$\phi_{(\cdot)}$ = electric potential due to $(\cdot)$, V
$\hat{\phi}$ = nondimensional electrostatic potential

I. Introduction

ON AVERAGE, a commercial aircraft is struck by lightning about once per year [1], out of which around 90% of these strikes are thought to be initiated by the aircraft itself [2–4]. Much of our knowledge of aircraft-triggered lightning is based on the data gathered by four major instrumented aircraft campaigns [5,6]: the Rough Rider project, involving an F-100F (Air Force Cambridge Research Laboratories, 1964–1966) [7,8]; the NASA storm hazards program, involving an F-106B (NASA, 1980–1986) [9–21]; the U.S. Air Force (USAF)/Federal Aviation Administration (FAA) lightning characterization program, involving a CV-580 (USAF/FAA, 1984–1985, 1987) [2,22–25]; and the French Transall program, involving a C-160 research aircraft (Office National d'Etudes et de Recherches Aérospatiales (ONERA), and Centre d'Essais en vol (CEV), 1984, 1988) [2,3,25]. These research aircraft were intentionally flown into thunderstorm regions to gather data on the aircraft–lightning interaction process (e.g., the NASA F-106B alone was struck by lightning 714 times [5]). Data gathered include electric field waveforms on the aircraft surface, current and current derivative measurements, electric and magnetic field derivatives on the aircraft surface, and high-speed video. Analysis of the data from the 1980s campaigns has elucidated the mechanisms of aircraft-triggered lightning, and the sequence of events preceding the strike is now well accepted [2,3,24].

This sequence of events is described in [2,3,5,24] and is summarized here for completeness. The first phase of the aircraft-initiated discharge begins when a conductive aircraft flies into a sufficiently high ambient field or is exposed to a rapid rise in the ambient field (e.g., due to nearby lightning [26]). Threshold ambient fields that triggered lightning for the CV-580 and C-160 research aircraft were around 50 kVm^{-1} [5]. In the presence of an ambient field, the aircraft becomes polarized, and the local electric field on the aircraft surface and its vicinity, at both the positive and negative ends, is amplified. This local electric field intensification can lead to the initiation of a bidirectional leader [24,27].

In all cases measured to date [5,6], a positive leader is initiated first since positive leaders are initiated and can propagate in lower electric fields than negative leaders. As the positive leader propagates in the direction of the electric field, it biases the potential of the aircraft to more negative values, and a few milliseconds later, when the negative fields on the aircraft are sufficiently magnified, a negative leader follows from an opposite extremity. The negative leader now travels in the direction opposite to the electric field. The typical sequential formation of positive and negative leaders is illustrated in Fig. 1.

This first phase of the bidirectional discharge, of which the aircraft is the center, is characterized by current pulses of amplitude ~1 kA (associated to stepped propagation of the negative leader), followed by a steady current component and a series of intracloud process pulses. This is the most common aircraft-triggered lightning event; when the aircraft is within a cloud, the positive leader propagates toward a negative cloud region, and the negative leader propagates towards a positive cloud region [28]. Although less common, aircraft can also initiate cloud-to-ground or cloud-to-cloud lightning when the aircraft is below or beside the cloud [1,25,29].

Even though this series of events is well accepted and understood, a quantitative physical model of the bidirectional leader initiation and propagation process [30,31] is still at an early stage of research [25,32,33]. Numerical models of aircraft-triggered lightning are due to [34–37] and can provide a quantitative assessment of the ambient electric fields that trigger lightning as well as the most likely leader initiation points. However, at this point, they lack predictive capability due to the complexity of the events at hand and the simplifications made in the models (in particular, the leader inception criteria are rough and not well established).

Currently, aircraft do not incorporate any means to reduce the risk of initiating the sequence of events described previously, and lightning avoidance primarily relies on rerouting aircraft trajectories to avoid dangerous thunderstorm regions [38]. In this work, we propose an active control system to reduce the risk of an aircraft-initiated lightning strike, which is based on the known asymmetry between the positive and the negative leaders. Section II deals with an analytical model of an ellipsoidal fuselage to introduce the strategy and provide a first estimate of its effectiveness. The theoretical study is then extended in Sec. III to a numerical evaluation of the concept on the Falcon aircraft geometry. Section IV discusses the practical implementation of the system, including the necessary sensors and actuators and their locations on the aircraft.

II. Analytical Model to Evaluate Net Charge Effect on First Leader Inception

An isolated conductive body in a region of high electric field becomes polarized, with one end becoming positively charged and the other end becoming negatively charged. This effect significantly enhances the electric field on the body's surface ranging from a factor of 2 (for a cylinder) or 3 (for a sphere) to approximately l/d for an elongated object of length l and diameter d. As the electric fields on the body and its vicinity intensify, localized streamer corona discharges can develop, and, if further stressed, the streamers may coalesce into self-propagating leader channels. In most cases, a positive leader would precede (Fig. 1) because the crucial breakdown field in air is known to be around twice as large for the negative leader as compared to the positive leader. If this were the case, it would be advantageous to artificially bias the body to a negative potential value (i.e., charge it negatively) to suppress the formation of the positive leader.

In this section, we present an analytical model to illustrate a charge control strategy that acts to delay the inception of the positive leader without triggering the negative leader in the process. We propose that the optimum net charge, in terms of lightning avoidance, corresponds to the level that keeps equal safety margins for the positive and negative discharges. The model also gives bounds to the applicability of the strategy and a measure of its effectiveness.

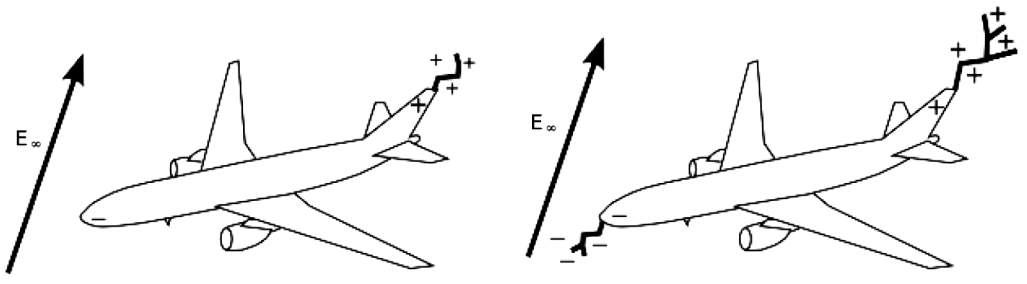

Fig. 1 Typical sequential formation of positive and negative leaders before the lightning strike: (left) positive leader initiation at T_0; (right) negative leader initiation at $T_0 + \sim 1$ ms.

A. Ellipsoidal Fuselage with Net Charge in External Field

The prestrike electrostatics of a conductive aircraft fuselage can be treated analytically using prolate spheroidal coordinates (ξ, η, φ). The aircraft fuselage is modeled as an ellipsoid, and its geometry is described by the shape factor ξ_0, or alternatively the aspect ratio λ,

$$\lambda = \frac{a}{b} = \frac{\xi_0}{\sqrt{\xi_0^2 - 1}}, \qquad \xi_0 = \frac{\lambda}{\sqrt{\lambda^2 - 1}} \tag{1}$$

where a and b are the semi-axes of the ellipsoid and c is its focal distance.

The ellipsoid can acquire a net charge Q [39] and is exposed to an ambient electric field $\boldsymbol{E}_\infty$ of arbitrary orientation. Exploiting the symmetry of the geometry, the external electric field is represented by a parallel component $E_{z,\infty}$, which is aligned with the axis of revolution of the ellipsoid (along z); and a transverse component, which is orthogonal to the axis of revolution of the ellipsoid, and its direction is taken along x, $E_{x,\infty}$.

Appendix A presents the electric potential and corresponding electric fields for the separate effects of a net charge Q (and no external field) and the separate components of the external electric field $\boldsymbol{E}_\infty$ (for an uncharged body). For the general case of a charged ellipsoid in an external field of arbitrary orientation, the electrostatic potential ϕ and the field components $\boldsymbol{E}$ can be obtained by superposition:

$$\phi = (\phi)_Q + (\phi)_{E_{z,\infty}} + (\phi)_{E_{x,\infty}} \tag{2}$$

$$\boldsymbol{E} = (\boldsymbol{E})_Q + (\boldsymbol{E})_{E_{z,\infty}} + (\boldsymbol{E})_{E_{x,\infty}} \tag{3}$$

The analytical formulas for the potential and field components in Eqs. (2) and (3) are listed in Table A1 in Appendix A.

In particular, Eq. (3) can be evaluated on the fuselage's surface to determine the normal fields on the body (since the ellipsoid is conductive, the tangential components are zero).

B. Criteria for Leader Inception Based on Surface Fields

A criterion for leader inception based on surface fields reaching the corresponding breakdown thresholds is used in this section. Positive and negative breakdowns will occur for $E_{\max} = E_{\text{cr}}^+$ and $(-E_{\min}) = E_{\text{cr}}^-$, respectively, where in general $E_{\text{cr}}^- = NE_{\text{cr}}^+$ ($N \approx 2$) due to the asymmetry in positive and negative leader inceptions. This simple criterion is selected to illustrate the application of the strategy without complicating the mathematical analysis. This criterion will be revisited in Sec. III, for a more realistic representation.

As we have seen [Eq. (3)], the electric fields on the surface of the body are given by a linear relationship of the form

$$\frac{\boldsymbol{E}_n}{E_\infty} = \boldsymbol{M} \begin{Bmatrix} \frac{\boldsymbol{E}_\infty}{E_\infty} \\ \bar{Q} \end{Bmatrix} \tag{4}$$

where $\boldsymbol{M}$ is a geometry-dependent matrix and $\bar{Q} = Q/4\pi\varepsilon_0 c^2 E_\infty$ is a dimensionless net charge. For a generic orientation of the external field, the location of the maximum and minimum surface fields as well as their values will need to be evaluated numerically.

C. Charge Control

We propose that the asymmetry between the positive and negative leader inception can be used to delay the onset of an aircraft-triggered lightning strike by controlling the net charge of the aircraft so that equal safety margins for the positive and negative discharges are kept.

For the case of a symmetric conductive body that is charged (net level Q) in the presence of a parallel field, $E_\infty = E_{z,\infty}$, the maximum and minimum surface fields will be given by

$$\begin{aligned} E_{\max} &= \beta E_\infty + \alpha Q, \\ -E_{\min} &= \beta E_\infty - \alpha Q \end{aligned} \tag{5}$$

where the coefficients α and β depend exclusively on the geometry of the body ξ_0, as shown in Appendix A. In this case, the location of these fields occurs at $\eta = \pm 1$, and the parameters α and β take the values (Table A2)

$$\alpha = \frac{1}{4\pi\varepsilon_0 c^2} \frac{1}{\xi_0^2 - 1} \tag{6}$$

$$\beta = \frac{1}{\xi_0^2 - 1} \frac{1}{\xi_0 \ln \sqrt{(\xi_0 + 1)/(\xi_0 - 1)} - 1} \tag{7}$$

Note that, in general, the situation without symmetry is more complex. In that case, the locations of the maximum and minimum fields will depend on the net charge level and the orientation of the external field, and so will α and β.

The charge control law will be such that we keep equal safety margins for the positive and negative discharges. Using the leader inception threshold defined in Sec. II.B,

$$E_{\text{cr}}^+ - E_{\max} = E_{\text{cr}}^- - (-E_{\min}) \tag{8}$$

For the case of fixed points of maximum and minimum fields, and geometry-dependent coefficients, this law can be easily obtained. Using the expressions for the maximum and minimum surface fields of Eq. (5), the optimum net charge in terms of lightning avoidance is

$$Q_{\text{opt}} = -\frac{1}{2\alpha}(E_{\text{cr}}^- - E_{\text{cr}}^+) \approx -\frac{E_{\text{cr}}^+}{2\alpha} \tag{9}$$

where, in the last equality, it has been assumed that $E_{\text{cr}}^- = 2E_{\text{cr}}^+$. Information about the geometry appears in the coefficient α, and information about the air properties, namely, density (i.e., flight altitude), appears in the breakdown field E_{cr}^+.

The proposed strategy can be applied until a bidirectional leader is incepted. This occurs when the breakdown thresholds are reached [null safety margins in Eq. (8)], which happens if the ambient field exceeds $(E_\infty)_{\max} = 3E_{\text{cr}}^+/(2\beta)$. This value is the highest external field that can be avoided using charge control.

For comparison, taking as a baseline an uncharged aircraft, $Q = 0$, the maximum and minimum fields on its surface become

$$E_{\max} = -E_{\min} = \beta E_\infty \tag{10}$$

and a positive leader will be incepted when the ambient field exceeds $(E_\infty)_{\max} = E_{\text{cr}}^+/\beta$. Therefore, by using the charge control strategy, the aircraft can fly safely through an external field 50% higher, as compared to a baseline uncharged case.

Note that an uncharged case is arbitrarily chosen as a baseline, to have some reference value for comparison. In reality, aircraft acquire net charge in flight from a number of sources including corona discharges, charged species in the engine exhaust, and charge transfer by collision with precipitation and particles in the atmosphere [40,41]. The charge acquired by aircraft can be ~1 mC [5], which is of the order of magnitude of the optimum charge levels predicted by our model, as we will see in Sec. III.C.4. Currently, modern aircraft have static dischargers that act to limit the charge buildup on the vehicle and control the location of corona discharges to isolate them and minimize their electromagnetic interference.

III. Concept Applied to Realistic Aircraft Geometry

The charge control strategy presented in Sec. II is extended here to a realistic aircraft geometry. The problem needs to be treated numerically, and we use the hybridizable discontinuous Galerkin method [42–44] to solve the prestrike electrostatics of a Falcon aircraft. Different criteria for leader inception are used, since a criterion based on the maximum surface fields (Sec. II.B) is sensitive to the mesh resolution. We estimate the effectiveness of the strategy by comparing the charge controlled to a baseline uncharged aircraft, for any possible orientation of the ambient field.

A. Prestrike Electrostatics of Falcon Aircraft

The prestrike electrostatics for any given aircraft geometry, in this case that of a Falcon aircraft, can be solved for any amplitude and orientation of the external field and net charge of the aircraft by the principle of superposition. Thus, only four problems need to be evaluated numerically to reconstruct the full space of solutions. Namely, a nondimensional Laplace equation for the electrostatic potential is solved using the following boundary conditions:

$$\hat{\nabla}^2\hat{\phi} = 0, \quad \boldsymbol{e} = -\hat{\nabla}\hat{\phi} \tag{11}$$

$$\begin{array}{lllll} \text{Net body charge:} & \hat{\phi} = 1 & \text{on aircraft;} & \hat{\phi} = 0 & \text{far field,} \\ \text{Field along } x\text{:} & \hat{\phi} = 0 & \text{on aircraft;} & \boldsymbol{e} = (1,0,0) & \text{far field,} \\ \text{Field along } y\text{:} & \hat{\phi} = 0 & \text{on aircraft;} & \boldsymbol{e} = (0,1,0) & \text{far field,} \\ \text{Field along } z\text{:} & \hat{\phi} = 0 & \text{on aircraft;} & \boldsymbol{e} = (0,0,1) & \text{far field} \end{array} \tag{12}$$

Let $\boldsymbol{e}_q, \boldsymbol{e}_x, \boldsymbol{e}_y$, and $\boldsymbol{e}_z$ be the electric fields computed by numerically solving the Laplace equation [Eq. (11)] with the previously mentioned boundary conditions [Eq. (12)], respectively. The total field $\boldsymbol{E}$ is obtained by superposition (for any point in the volume and on the aircraft's surface),

$$\boldsymbol{E} = \frac{Q_{\text{ac}}}{R_f C}\boldsymbol{e}_q + E_\infty(\sin\theta\cos\varphi\boldsymbol{e}_x + \sin\theta\sin\varphi\boldsymbol{e}_y + \cos\theta\boldsymbol{e}_z) \tag{13}$$

where the orientation of the ambient field with respect to aircraft axis (θ, φ) is pictured in Fig. 2, Q_{ac} is the net charge of the aircraft, R_f is the fuselage radius used as the reference length, and C is the self-capacitance of the aircraft that only depends on its geometry and can be evaluated numerically. From these solutions, the polarization of the aircraft as well as the electric field amplification on the aircraft's surface and its vicinity can be obtained for any external field and net charge, Fig. 3.

B. Leader Inception Threshold Based on Critical Charge

The criterion based on comparing the maximum surface fields to threshold values (Sec. II.B) gave mesh-dependent results, as expected, and so was discarded for this part. In this section, we use the approach developed by ONERA and the University of Padova [35–37], which is based on the critical charge concept of [45].

The events preceding leader formation have been studied both experimentally in the laboratory [46,47] and theoretically [45,48]. It is well accepted that, before positive leader formation, an impulse streamer corona forms, and, at its root, a short bright stem is observed. Gallimberti [45] proposed that a leader forms as the result of a thermal-ionization instability once the stem surpasses a critical temperature of around 1500 K.

Incorporating such a condition to predict leader inception into our prestrike aircraft electrostatic model (Sec. III.A) would require simulating very detailed gas-discharge physics. Fortunately, [45,49] transformed this thermodynamic criterion into an electrostatic condition (a critical charge). Many others have used criteria based on the critical charge concept to predict leader inception [50–54].

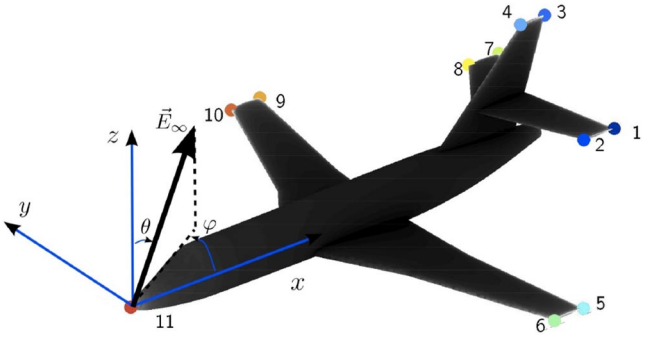

Fig. 2 Falcon aircraft in external electric field. Select points for evaluation of leader inception criteria.

For an estimate of this critical charge, Gallimberti's model [45] can be evaluated analytically. Assuming a cylindrical plasma channel representing the stem with a constant number of molecules per unit length ($\pi r^2 n = \pi r_0^2 n_0$), the energy balance becomes

$$\frac{d(\pi r^2 nh)}{dt} = fEI \tag{14}$$

where h is the thermal enthalpy (7/2kT, for a diatomic gas), f is the fraction of energy that goes to gas heating, and EI is the Joule power. Assuming the electric field within the corona is constant E_{cr} (which is the usual assumption for a streamer corona) and writing the current in terms of the rate of change of the charge, $I = dQ/dt$, the critical charge required to heat the gas to a critical temperature T_{cr} from a reference condition T_0 becomes

$$Q_{\text{cr}} = \frac{7\pi k n_0 r_0^2 (T_{\text{cr}} - T_0)}{2fE_{\text{cr}}} \tag{15}$$

Using the values quoted by Galliberti [45]: $r_0 = 0.1$ mm, $E_{\text{cr}}^+ = 450$ kV/m, $T_{\text{cr}} = 1500$ K, and $f = 0.1$, ambient temperature and atmospheric pressure: $Q_{\text{cr}}^+ \approx 1$ μC, which is the value that is used by many researchers [50,53].

This model is reasonable for a positive leader in which the sequence of events that precedes leader inception is first the streamer corona, then the heating of the stem, then the leader. For the negative leader, the situation is more complex. However, experimental results [47,55] show that an equivalent critical charge for the negative leader is approximately four times higher than for the positive leader. Here, we will use $Q_{\text{cr}}^-/Q_{\text{cr}}^+ = 4$.

The basic leader-initiation thresholds used by the model are the critical fields and charges of the corona, $E_{\text{cr}}^\pm$, $Q_{\text{cr}}^\pm$, which have been determined from laboratory measurements. When considering aircraft-triggered lightning, there are certain differences that are not accounted for at present. First, analysis at different altitudes would need to consider the scaling with density of these parameters. Using the classical scaling laws, $E_{\text{cr}}^\pm \propto n_0$ and $Q_{\text{cr}}^\pm \propto n_0^{-2}$ [55], as obtained from Eq. (15) using $r_0 \propto n_0^{-1}$. Second, natural lightning occurs in much longer length scales than laboratory sparks. Third, laboratory setups are associated with static electrodes, whereas a fast-moving aircraft can escape regions of space charge, created by local corona phenomena, modifying the conditions for leader formation (e.g., it has been observed that initiation of upward leaders from rotating blades of windmills occurs more readily than from static towers [56]). In addition, the effect of the rate of rise of the electric field for nonstatic conditions is also expected to have an impact in the leader initiation criteria. Since all of these effects will likely affect the positive and negative polarities in similar ways, and we are mainly interested in the asymmetry between both, they are not expected to have a major impact in the conclusions drawn. However, they will most likely impact the absolute values of the breakdown ambient fields computed. For the results presented in this Paper, sea-level conditions are assumed, and the effects of wind are neglected in the criteria for leader formation.

Several approximations to estimate the charge produced by the corona using the Laplacian solution of the field (which necessarily ignores any presence of charge) have been proposed based on geometrical constructions for a constant electric field corona [49,52–54,57–60]. We tested several methods, including a volumetric integration of the charge [53], and used an approximation based on surface integrals [36] for the results presented in Sec. III.C.3. The selection of the approach was driven by computational speed [36] and is outlined here:

1) Find connected regions on the aircraft's surface for which $E_n > E_{\text{cr}}$; this is the corona zone Σ_c.

2) Integrate the surface fields in Σ_c to estimate the local corona charge: $Q = \int\int_{\Sigma_c} \varepsilon_0 E_n \, \mathrm{d}S$.

3) The leader inception criterion is set as $Q \geq Q_{\text{cr}}$.

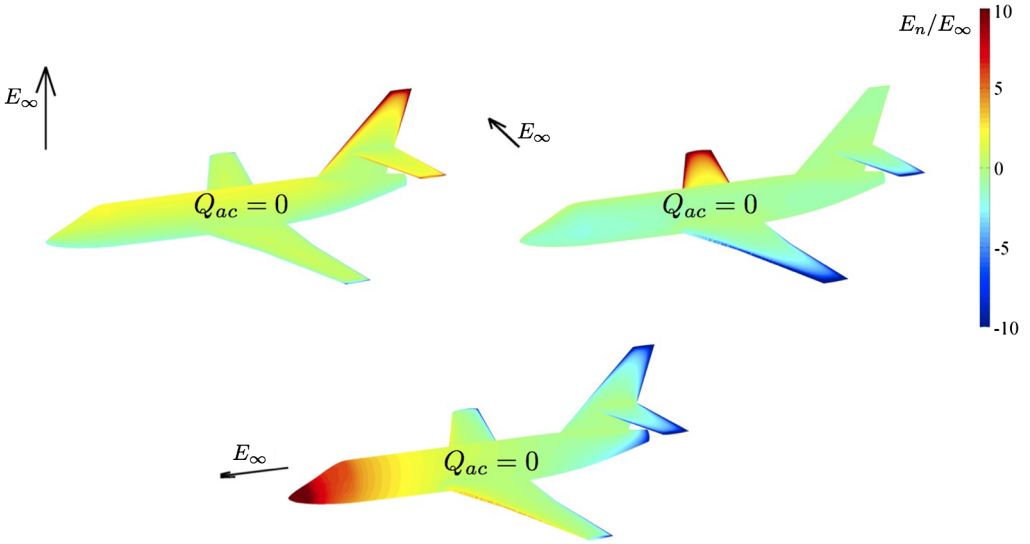

Fig. 3 Uncharged aircraft polarization and surface fields as a function of field orientation.

Since the leader inception criterion is now based on a surface integral (instead of a point measurement), there is very little dependence on the mesh size.

To avoid integrating over very large surface areas that are not realistic, we have limited the size of the integration regions by a maximum distance to the center point of Σ_c, d. Practical independence of the results with d is achieved for

$$d/R_f > \max\left(\sqrt{\frac{Q_{\rm cr}^+}{\epsilon_0 E_{\rm cr}^+ \pi}}, \quad \sqrt{\frac{Q_{\rm cr}^-}{\epsilon_0 E_{\rm cr}^- \pi}}\right) \cdot R_f^{-1} \tag{16}$$

which, using the parameters defined in Sec. III.C.3, translates to $d/R_f > 0.35$ (the negative discharge is more critical). A value of $d/R_f = 0.75$ was chosen for the results presented in this Paper.

Note that the critical corona charge criterion assumes a preexisting corona. In reality, corona inception also needs to be tested. Criteria for corona inception require that the number of electrons produced in an avalanche initiated by a single electron exceeds a certain threshold [61] and typically require local fields above 30 kV/cm at atmospheric pressure. As in [36], it is assumed here that local geometric features at a scale not resolved provide a sufficient amplification within Σ_c to initiate a corona.

C. Effectiveness of Charge Control Strategy

Of interest to us is evaluating the effectiveness of the charge control strategy, measured as the increase in the ambient field that triggers a lightning strike, when comparing an optimally biased aircraft to an uncharged baseline case.

1. First Leader Inception: Calculation of External Field Amplitude and First Attachment Point

In what follows, we define the algorithm used to estimate the external field amplitude that triggers the lightning strike, as well as the first attachment point, based on the methods of [35–37]. Contrary to [35–37], which assume the first leader is always positive, we test both positive and negative leader formations. For a fixed orientation of the ambient field (θ, φ) and net charge of the aircraft $Q_{\rm ac}$, we perform the following steps:

1) Initialize the amplitude of the external field to a low value E_∞^0.

2) Solve the electrostatic problem for this amplitude by superposition, Eq. (13).

3) For the most likely possible attachment points (1–11) on the aircraft surface, Fig. 2, test the leader inception criterion based on critical charge defined in Sec. III.B. Note that the values for $Q_{\rm cr}$ and $E_{\rm cr}$ differ in the positive and negative surfaces of the aircraft. At the positive surfaces, inception of a positive leader needs to be tested. At the negative surfaces, inception of a negative leader needs to be tested.

4) If a leader is incepted (of either polarity), the point where it occurs is the first attachment point, and the amplitude of the external field considered is the one that triggers the strike.

5) If no leaders are incepted, increase the amplitude of the field E_∞ (by 0.1%), and return to step 2.

2. Optimally Biased Aircraft: Breakdown Condition

Since the charge control strategy drives the aircraft potential toward the value that ensures equal likelihood of positive and negative leader formation, at the point of breakdown, both leaders are incepted simultaneously. This condition is used to compute the limit of the charge control strategy by modifying the algorithm in Sec. III.C.1 to determine the optimum charge, for a fixed orientation of the ambient field (θ, φ):

1) Initialize the amplitude of the external field to a low value E_∞^0 and the net charge of the aircraft $Q_{\rm ac}^0$.

2) Solve the electrostatic problem for this amplitude and net charge by superposition, Eq. (13).

3) Estimate the corona charge Q_i ($i = 1$–11) at the most likely attachment points on the aircraft surface, Fig. 2. Find the point most likely to incept a positive leader $\max(Q_i)$ and the point most likely to incept a negative leader $\min(Q_i)$.

4) Increase the amplitude of the field E_∞^1 until a leader (of either polarity) is incepted based on the algorithm defined in Sec. III.C.1.

5) Determine whether simultaneous inception of the positive and negative leaders is likely. If $|\max(Q_i)/Q_{\rm cr}^+ + \min(Q_i)/Q_{\rm cr}^-| \le \epsilon$, with $\epsilon \ll 1$, then both leaders are equally likely, and the optimum condition has been found. Otherwise, increase the charge of the aircraft to

$$Q_{\rm ac}^1 = Q_{\rm ac}^0 - \text{sign}[\max(Q_i)/Q_{\rm cr}^+ + \min(Q_i)/Q_{\rm cr}^-]\delta Q \tag{17}$$

with δQ taken as 1 μC.

6) Return to step 2 using $Q_{\rm ac}^0 = Q_{\rm ac}^1$ and $E_\infty^0 = E_\infty^1$.

3. Numerical Results

The effectiveness of the strategy has been estimated assuming the following parameters for leader inception: $E_{\rm cr}^+ = 450$ kV/m, $E_{\rm cr}^- = 750$ kV/m [49], $Q_{\rm cr}^+ = 1$ μC, and $Q_{\rm cr}^- = 4$ μC [47,55]. These values are reported in the literature for laboratory conditions (atmospheric pressure). The analysis is therefore representative of sea-level conditions.

The Falcon geometry used is shown in Fig. 2, in which the reference length is the radius of the fuselage $R_f = 1.25$ m and the self-capacitance is $C = 839.5$ pF. To evaluate all possible

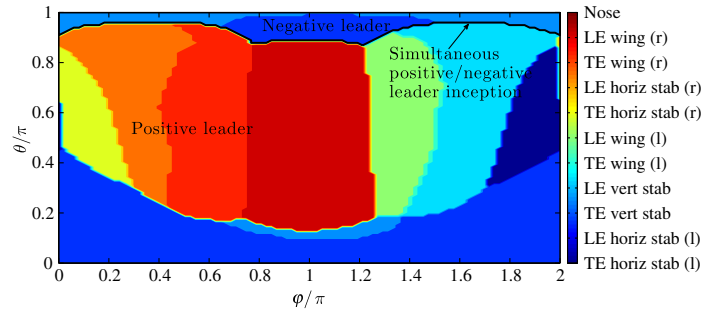

a) Baseline case, $Q_{ac} = 0$: first attachment

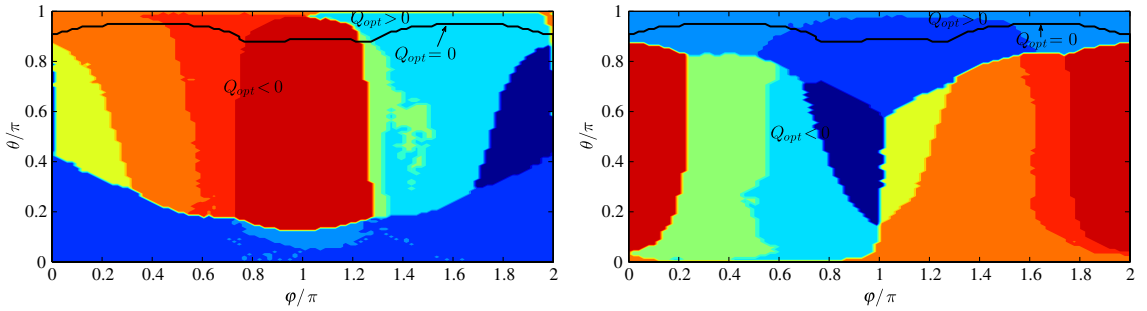

b) Optimal aircraft charging: positive attachment

c) Optimal aircraft charging: negative attachment

Fig. 4 Attachment points for baseline and optimal charging. Color code coincides with that of Fig. 2: TE refers to trailing edge; LE is the leading edge; (l, *r*) refers to the left and right sides of the aircraft, respectively (aircraft reference frame); horiz stab is the horizontal stabilizer; vert stab is the vertical stabilizer; and wing location is at the tip. Each point corresponds to a different orientation of the ambient field, as defined in Fig. 2.

orientations of the external field, the relative orientation of the field with respect to aircraft axis has been varied in the range $\theta = [0, \pi]$, $\varphi = [0, 2\pi)$, since $E(-\theta, \varphi) = E(\theta, \varphi + \pi)$. Note that in reality φ would only need to be evaluated in the range $\varphi = [0, \pi)$ since the aircraft is symmetric with respect to $y = 0$ (left/right symmetry).

Figure 4a shows the first attachment point for the baseline case, $Q_{ac} = 0$. The color code is shown in Fig. 2, but the legend is labeled with the attachment points for easy reference. The left/right symmetry can be appreciated with respect to $\varphi = \pi$. Note that some lack of symmetry is observed since the conditions for attachment at the leading and trailing edges of the different elements (e.g., wing tips) are very similar; the slight difference left/right is due to numerical effects (Figs. 4 and 5). The black envelope corresponds to simultaneous triggering of the positive and negative leaders; below the envelope, the positive leader is incepted first, and above the envelope, the negative leader precedes. As expected, in the majority of cases, the positive leader is initiated first. However, when the electric field is downward ($\theta \approx \pi$), triggering of the negative leader from the vertical stabilizer is more likely.

For the optimally biased aircraft, at breakdown, both leaders are incepted simultaneously. Figure 4b shows the positive attachment point, and Fig. 4c shows the negative attachment point. The optimum charge at breakdown, for the parameters considered, is pictured in Fig. 5a. In this case, the black envelope corresponds to the optimum net charge of the aircraft being zero, and it is the same as the black envelopes in Fig. 4 (simultaneous positive and negative attachments). Below the envelope, the optimum net charge needs to be negative (since for an uncharged aircraft the positive leader is incepted first); above the envelope, the optimum net charge needs to be positive (since for an uncharged aircraft the negative leader is incepted first). For most orientations, a negative net charge is preferred. A zero net charge is only desirable for select orientations of the electric field (in the vicinity of a vertical field pointing downward $\theta \approx \pi$). There is also a region in the vicinity of ($\varphi/\pi \approx 3/4$, $\theta/\pi \approx 0.2$), and by symmetry ($\varphi/\pi \approx 5/4$, $\theta/\pi \approx 0.2$), where the optimum net charge is very small (red-orange wings in Fig. 5a). In this vicinity, there is risk of negative attachment if the aircraft acquires some negative charge. For this orientation, the field is pointing into the right side of the aircraft, and the negative leader would be incepted from the trailing edge of the right wing tip (trailing edge of the left wing tip for $\varphi/\pi \approx 5/4$), Fig. 4c.

Comparing the breakdown fields predicted for the optimally charged aircraft $E_{\infty}^{Q_{opt}}$ and for the uncharged baseline $E_{\infty}^{Q=0}$, the effectiveness of the strategy is measured as

$$\left(E_{\infty}^{Q_{opt}} - E_{\infty}^{Q=0}\right)/E_{\infty}^{Q=0} \tag{18}$$

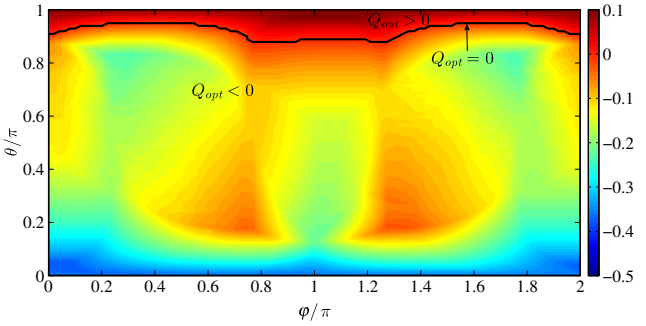

a) Aircraft optimum charge, in mC

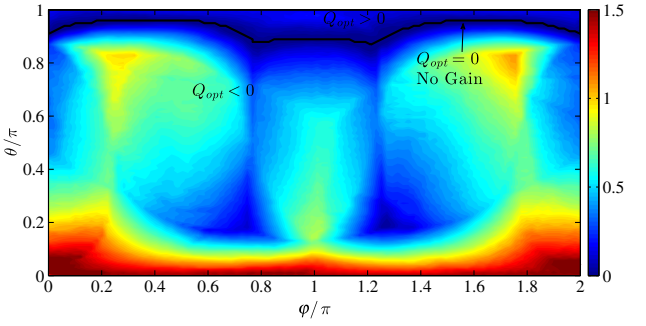

b) $\left(E_{\infty}^{Q_{opt}} - E_{\infty}^{Q=0}\right)/E_{\infty}^{Q=0}$

Fig. 5 Aircraft optimum charge and effectiveness of the charge control strategy. Each point corresponds to a different orientation of the ambient field, as defined in Fig. 2. The black envelope corresponds to a) the optimum net charge being zero and b) no gain (since the baseline case for comparison is the uncharged aircraft).

and is shown in Fig. 5b. As for the ellipsoidal geometry, there is a clear advantage when flying at the optimally charged condition as compared to flying uncharged. The gain depends on the relative orientation of the external field; there is no gain when the optimal charge is zero (field pointing close to downward), and the maximum gain occurs when the field points upward ($\theta \approx 0$). A field pointing upward is representative of a cloud-to-ground strike, since the cloud base is often negative with respect to the ground, and the gain here is a factor of ∼2.5 (as a result of the very exposed empennage).

Note that Fig. 5b (effectiveness) is a mirror image of Fig. 5a (optimum charge). Maximum effectiveness is obtained for orientations that require highest optimal charge (in magnitude), since this corresponds to the largest deviation from the baseline case $Q_{ac} = 0$.

4. *Discussion of Numerical Results*

The model uses several parameters that are not precisely known or are approximate values. The corona stability fields $E_{cr}^{+} \approx 450$ kV/m and $E_{cr}^{-} \approx 750$ kV/m are fixed in this analysis, since these values are quoted repeatedly in the literature (atmospheric conditions). However, the values of the critical corona charge Q_{cr}^{+} and the ratio of Q_{cr}^{+}/Q_{cr}^{-} are not accurately known. As will be shown, the choice of these parameters guides the amplitude of the external inception fields (depends on Q_{cr}^{+}) and the asymmetry encountered between the positive and the negative leaders (defined by Q_{cr}^{-}/Q_{cr}^{+}).

The effect of the choice of the critical corona charge (positive polarity) Q_{cr}^{+} is explored in what follows. All other parameters remain unchanged, and the critical corona charge of negative polarity is adjusted to maintain the ratio $Q_{cr}^{-}/Q_{cr}^{+} = 4$ and thus the asymmetry of leader inception.

The first observation is that the location of the first attachment point (both for the zero net charge and optimum charge conditions) is only slightly affected by the choice of Q_{cr}^{+}. Illustrative of this observation is that the probability of first attachment to the different regions of the aircraft is practically unchanged when Q_{cr}^{+} varies in the range 1–15 μC, Table 1. Here, the probability is estimated assuming all orientations of the external field are equiprobable and the 1–11 points are grouped into general zones: nose (11), wing tips (5, 6, 9, 10), vertical stabilizer tips (3, 4), and horizontal stabilizer tips (1, 2, 7, 8).

Figure 6 shows the mean and standard deviation of the breakdown ambient fields, optimum charge, and gain, assuming equiprobability of the ambient field orientations, as a function of the critical corona charge Q_{cr}^{+}.

The critical corona charge drives the amplitude of the ambient field that triggers breakdown. As the critical corona charge is increased, the critical ambient fields for leader inception (both for positive and negative polarity) increase as shown in Fig. 6a. These dependencies are close to linear with the critical corona charge. Since this parameter has a similar effect on strike onset with and without active control, the effectiveness of the strategy presents a much weaker dependency with Q_{cr}^{+}. The ratio between the breakdown ambient field using charge control to the breakdown field of an uncharged aircraft presents a much smaller dependency with Q_{cr}^{+} than either separately, as shown in Fig. 6b. Thus, despite the uncertainty in the model parameters, the results in Fig. 6b give us confidence in the claimed effectiveness of the strategy: for the range considered, the aircraft can fly safely through ambient fields that are ∼50% higher when using charge control.

Table 1 Impact of choice of Q_{cr}^{+}: case $Q_{ac} = 0$ (baseline)

	Probability of attachment, %			
Q_{cr}^{+}, μC	Nose	Wing	Vertical stabilizer	Horizontal stabilizer
1	18	41	32	9
2	19	43	28	10
3	20	41	29	10
4	22	41	27	11
5	22	41	27	10
7	23	41	27	9
10	23	42	27	8
15	22	42	28	7

Despite the interest of using charge control, implementation of the strategy would require a precise knowledge of the optimum net charge of the aircraft, which currently cannot be determined due to the uncertainty in the model's parameters. In particular, the optimum net charge of the aircraft is proportional to Q_{cr}^{+} as shown in Fig. 6c.

The other parameter that deserves our attention is the ratio Q_{cr}^{-}/Q_{cr}^{+}. In what follows, all other parameters remain unchanged, and the critical corona charge of positive polarity is kept at 1 μC.

The ratio Q_{cr}^{-}/Q_{cr}^{+} (along with E_{br}^{-}/E_{br}^{+}) controls the degree of asymmetry between the positive and the negative leaders. Therefore, the choice of these parameters has a large impact on the evaluation of the charge control usefulness. The ratio of $Q_{cr}^{-}/Q_{cr}^{+} = 4$ was taken from experimental data of [47,55] as a first estimate, but there is uncertainty associated with this choice. In what follows, we estimate the impact of this ratio on the results by varying this parameter in the range $Q_{cr}^{-}/Q_{cr}^{+} = (0.6, 1, 2, 3, 4, 5)$.

For the baseline case ($Q_{ac} = 0$), above a certain degree of asymmetry $Q_{cr}^{-}/Q_{cr}^{+} \sim 2$, the polarity of the first leader and its attachment point remain pretty much unchanged. The reason is that, as shown in Fig. 4a, the positive leader precedes in most instances, and since the value of Q_{cr}^{+} has been fixed to 1 μC, the numerical solution for $Q_{ac} = 0$ in the region where the positive leader is incepted first is unchanged by the choice of Q_{cr}^{-}/Q_{cr}^{+}. The solution for the optimum charge is of course affected by the choice of Q_{cr}^{-}/Q_{cr}^{+}, and the higher this parameter, the higher the predicted effectiveness, Fig. 7. For lower values of Q_{cr}^{-}/Q_{cr}^{+}, the region in which the negative leader precedes is significantly larger, as a result of the reduced asymmetry between polarities.

Some other details of the influence of aircraft net charge on the probability of lightning initiation from aircraft were presented in [62]. Note that convergence and independency of the results with the numerical mesh was demonstrated for all the results presented in this Paper.

IV. Practical Implementation

Even though a practical implementation of the strategy would require a significant improvement on the state of the art in the prediction of leader inception, in this section, we discuss the different elements involved in the system [63] as well as some practical limitations detected. A schematic of the envisioned implementation is shown in Fig. 8.

A. Monitoring the Electrical Environment

The proposed strategy relies on knowledge of the external field (amplitude and orientation) as well as the net charge of the aircraft. These can be retrieved from local electric field measurements with onboard electric field sensors placed on select aircraft surfaces; see Fig. 8. In the figure, the sensors are marked by rectangles, and the arrows indicate the electric field sensors' orientations. Typical electric field sensors used on aircraft are rotating shutter field meters, called electric field mills, or mills [64]. At least four electric field sensors are required to be able to determine the three spatial components of the external vector electric field plus the net aircraft charge from the electric fields measured by the sensors, but at least six sensors are preferred for better accuracy [65]. The location of the electric field sensors needs to be selected to unambiguously determine the external field and net aircraft charge [66]; an example placement of the electric field sensors, recommended by [65], is shown in Fig. 8. The information from the measurements can then be used to retrieve the external electric field and aircraft net charge from a previously calibrated matrix (which depends on the aircraft geometry and the location of the sensors). Possible algorithms and calibration procedures have been reported in the literature [64,65,67]. Other types of electric field sensors are proposed in the literature, e.g., radioactive probes and corona points [68], or electric field whistles [69].

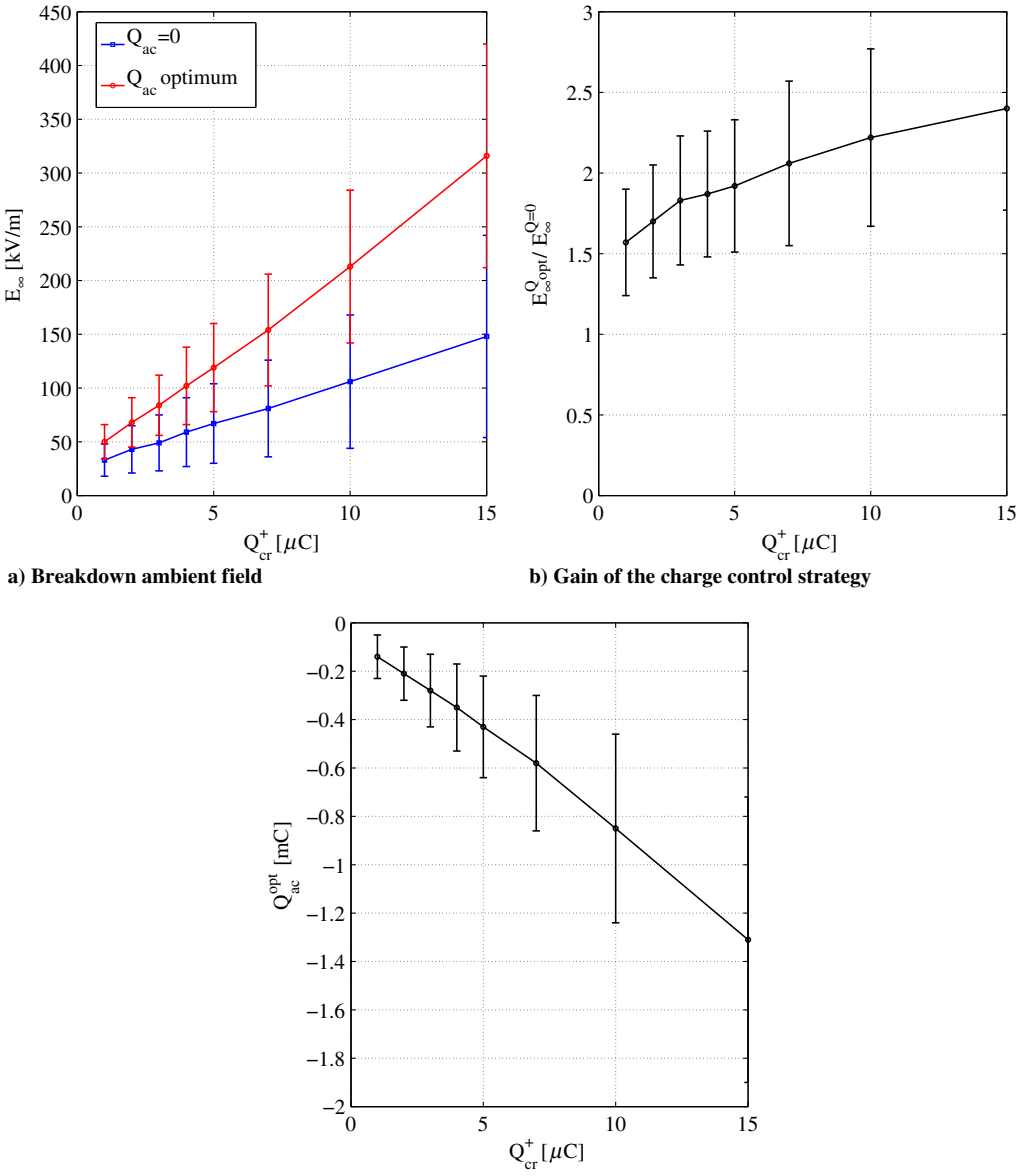

Fig. 6 Breakdown ambient field for baseline and optimum charging, gain of the charge control strategy ($E_\infty^{Q_{opt}}/E_\infty^{Q=0}$), and optimum charge for limiting condition as a function of the critical corona charge Q_{cr}^+. Equiprobability of ambient field orientation has been assumed. Negative level satisfies $Q_{cr}^-/Q_{cr}^+ = 4$.

B. Net Charge Modification Through Ion Emission

The modification of the net charge of the aircraft could potentially be achieved by emission of charge of opposite polarity from the aircraft surface [70].

Successful aircraft charging using ion emission has been achieved before using high-voltage stinger probes producing coronas [41,67,71]. In these references, an onboard high-voltage power supply (of the order of 1–10 kV) is used, with the high-voltage terminal connected to a cable that terminates in a point or brush that produces a corona discharge exposed to the airstream. The low-voltage terminal is connected to the airframe of which the potential is to be controlled [41]. The currents emitted by each one of these emitters are of the order of 10 μA but can be increased through the geometry of the exposed electrode, the number and separation of the filaments in the brush, or the level of voltage applied.

Regarding requirements on the ion emitters, the optimum net charge levels for a Falcon aircraft were estimated in Sec. III.C.4 on the order of 0.1–1 mC for a wide range of conditions (typically of negative polarity). A typical airliner flies about 250 m in 1 s, and this may be of the order of the motion required to enter the area of influence of a cloud charge center. If a 1 s charge-evacuation time is assumed, the current required is 100–1000 μA. Moreover, if the potential bias for emission is ~10 kV (for a corona emitter), the required power is of the order of 1–10 W.

In addition, it is well known that electric fields in thunderclouds can change abruptly due to lightning discharges. Intracloud and cloud-to-ground discharges are known to sometimes initiate upward positive leaders from ground objects [26]. Therefore, these abrupt electric field changes are also expected to initiate leaders from aircraft. It will need to be determined whether this additional source of lightning can be mitigated using the charge control system; i.e., the most probable limitations will be related to limitations in the charge-evacuation times and the speed of the track-and-respond system, and this might decrease the percentage of lightning strikes that are avoided using charge control.

Appendix B uses the ellipsoidal model of a fuselage, described in Sec. II and Appendix A, to illustrate the feasibility of artificial charging using ion emission. In particular, ions emitted from the aircraft are affected by the wind and the electric field, so the ion emitters need to be located to favor evacuation of the ions and ensure that they do not return attracted by the oppositely charged regions of the aircraft.

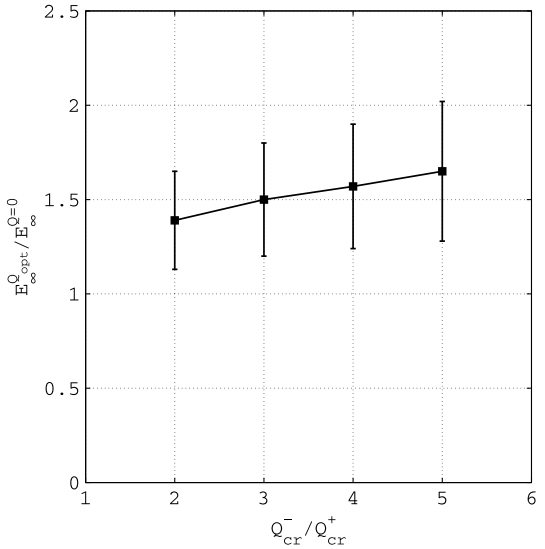

Fig. 7 Gain of the charge control strategy $E_\infty^{Q_{opt}}/E_\infty^{Q=0}$ as a function of the degree of asymmetry Q_{cr}^-/Q_{cr}^+. Equiprobability of ambient field orientation has been assumed. Critical positive corona charge is kept at $Q_{cr}^+ = 1\ \mu$C.

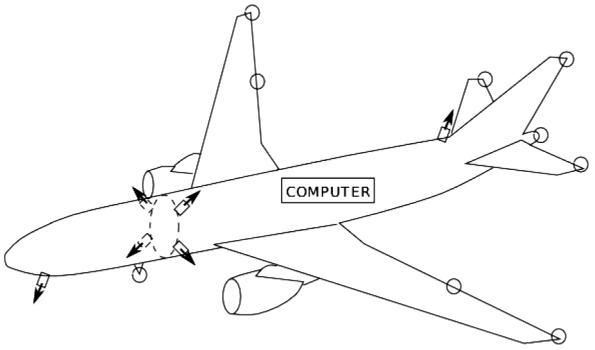

Fig. 8 Schematic of the envisioned implementation of a charge control strategy for airplane-triggered lightning strike risk reduction. Ion emitters are marked by circles, and electric field sensors are marked by rectangles, with the arrows indicating their orientation.

In general, to minimize the probability of ion return upon emission, positive ions must be emitted from the positive side of the aircraft; whereas negative ion emission needs to occur from the negative end. An important observation from the model in Appendix B is that, as the aircraft is biased toward the optimum charge condition (e.g., negative), the region from which (positive) ions can be emitted becomes smaller. Thus, the ion emitters should be placed in locations where the amplification of the field, and thus the surface charge, is maximized, which corresponds to regions of small radius of curvature.

In addition, ion trajectories will be affected by the wind parameter $\bar{U} = U_\infty/\mu_i E_\infty$, which measures the relative contribution of the wind U_∞ and the electric drift $\mu_i E_\infty$ (with μ_i the ion mobility).

As shown in Appendix B, in most cases, the ion trajectories will be dominated by the wind. This situation presents an additional limitation to the strategy: if the wind opposes and is larger than the electric drift, ion emission will be very difficult; e.g., positive ion emission might be hampered when flying into negative areas. In general, ion emission will be facilitated from the downstream extremities of the aircraft body, through a combination of flow and smaller radius of curvature effects. For the example presented in Fig. B1, the point of emission should be the tail cone.

Note that, in view of the strong wind influence, future work should investigate the effect of wakes and boundary layers on ion evacuation.

All in all, ion emitters should be preferentially placed at the downstream extremities of the aircraft, as shown in Fig. 8: large antenna blades, trailing edges of wing tips, trailing edges of vertical and horizontal stabilizer tips, and the tail cone. The electrical repulsion forces combined with the sweeping of the airflow will reduce the possibility of ion return to the aircraft and thus facilitate the ion evacuation process.

C. Controller

The charge control system requires an onboard controller that uses the information provided by the sensors to command the actuators. From the inferred instantaneous external field and aircraft net charge (Sec. IV.A), the likelihood of positive and negative leader inception from corresponding select aircraft surfaces will need to be determined. From this information, the optimum net charge of the aircraft required to keep equal safety margins for the positive and negative discharges, thereby reducing the likelihood of a lightning strike, can be estimated. Corresponding actuators, as described in Sec. IV.B, will need to be activated to force this optimum charge condition.

For an example, suppose that the onboard algorithms indicate that there is an $X\%$ safety margin for the positive discharge (i.e., an increase of $X\%$ in the ambient field would trigger a positive leader from the positive end of the aircraft) and a $3X\%$ safety margin for the negative discharge (i.e., an increase of $3X\%$ in the ambient field would trigger a negative leader from the negative end of the aircraft). In this situation, the controller would command the activation of positive charge emission until the onboard algorithms indicate equal safety margins $Y\%$ for both the positive and negative leaders. Necessarily, Y is greater than X and smaller than $3X$, due to the asymmetry of the leaders, thus reducing the likelihood of a lightning strike.

Note that this strategy relies on a continuous monitoring and actuation during flight (at a certain sampling rate) in order to account and compensate for 1) the inherent charging and discharging of the aircraft via its engine exhaust, onset of corona discharge, or from flying in and out of precipitation, and 2) gradual variations in the ambient field, due to the aircraft's motion, as well as rapid ambient field changes because of natural lightning, to the extent the control system is able to track and respond to these sources of variation.

Ultimately, the deployment of electric field sensors on aircraft (Sec. IV.A) could also be beneficial to assess the environmental conditions for aircraft-triggered lightning to occur (namely, ambient electric fields and aircraft net charge as well as correlation to flight altitude, weather, etc.). In addition, the strategy could be complemented by using the estimation of the ambient field and net charge of the aircraft to avoid dangerous conditions (i.e., ambient fields above certain thresholds, which would be a function of the accumulated net charge, e.g., $\sim$30 kV/m) to the extent the aircraft can maneuver.

V. Conclusions

Lightning strikes to aircraft are a fairly common risk that costs aircraft manufacturers millions of dollars annually. According to estimates from the National Oceanic and Atmospheric Administration, lightning is responsible for around \$2 billion annually in commercial airline operating costs and passenger delays, to which repair costs need to be added. Currently, the only risk-reduction measure available is based on rerouting aircraft trajectories, as informed by the weather radar and communications with ground and between pilots. This Paper has proposed an active measure to reduce the risk of an aircraft-initiated lightning strike based on the known asymmetry between positive and negative leader inception.

This charge control strategy is worth investigating in more detail since our estimates indicate that the aircraft would be able to fly safely through ambient fields that are around 50% higher than those of the uncharged baseline. A simple analytical model of a fuselage was used to explain the concept, and numerical simulation demonstrated that similar conclusions apply to a realistic aircraft geometry. Even though the effectiveness of the strategy is very promising, actual implementation will require a significant improvement in the prediction of the positive and negative leader inception.

Future work will need to confirm this Paper's hypothesis experimentally, by demonstrating that higher external fields are required to initiate lightning from a floating object when it is optimally charged as compared to uncharged. These experiments will also help clarify whether the theoretically estimated 50% increase in the electric field in which an aircraft could fly without initiating lightning is realistic given the assumptions and uncertainties in the calculations. In addition, experiments of aircraft charge control using ion emission are underway. Moreover, implementation of the strategy can benefit from theoretical advances in leader inception prediction.

Appendix A: Prestrike Electrostatics of Ellipsoidal Fuselage

Let us consider a prolate spheroid, which represents a conductive aircraft fuselage, in the presence of an external field. The external field can take any orientation, and the ellipsoid can acquire a net charge. The coordinates suitable to analyze this problem are axisymmetric prolate spheroidal coordinates (ξ, η, φ) related to the cartesian coordinates (x, y, z) by

$$\frac{x}{c} = \sqrt{(\xi^2 - 1)(1 - \eta^2)}\cos\varphi \tag{A1}$$

$$\frac{y}{c} = \sqrt{(\xi^2 - 1)(1 - \eta^2)}\sin\varphi \tag{A2}$$

$$\frac{z}{c} = \xi\eta \tag{A3}$$

where $\xi \in [1, \infty)$, $\eta \in [-1, 1]$, and $\varphi \in [0, 2\pi)$. The coordinates are shown in Fig. A1, in which R is the cylindrical radius, $R = \sqrt{x^2 + y^2}$. Surfaces of constant ξ are ellipsoids of revolution with focal distance c and semi-axes:

$$a = c\xi, \qquad b = c\sqrt{\xi^2 - 1} \tag{A4}$$

In these coordinates, the fuselage can be described by the parameter ξ_0, or alternatively the aspect ratio $\lambda = a/b$, given by Eq. (1).

The electrostatic solution, before a lightning strike, can be obtained by solving Laplace's equation for the electrostatic potential ϕ,

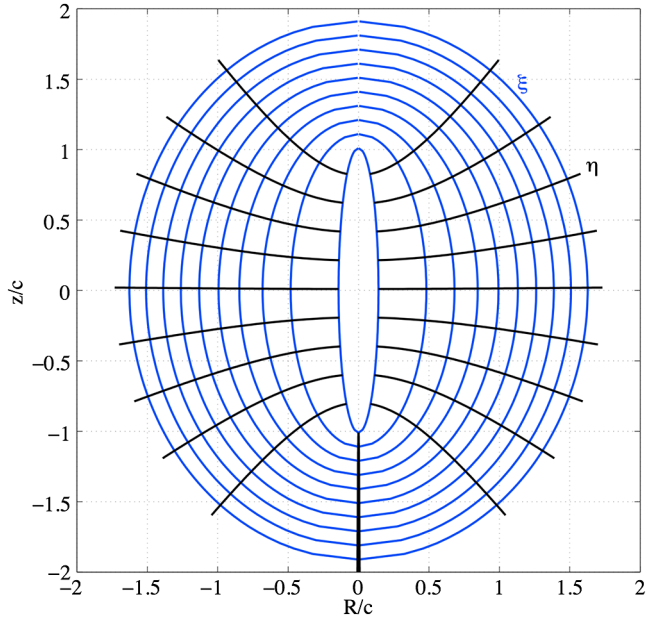

Fig. A1 Prolate spheroidal coordinates.

$$\frac{1}{c^2(\xi^2 - \eta^2)}\left\{\frac{\partial}{\partial\xi}\left[(\xi^2 - 1)\frac{\partial\phi}{\partial\xi}\right] + \frac{\partial}{\partial\eta}\left[(1 - \eta^2)\frac{\partial\phi}{\partial\eta}\right]\right\} + \frac{1}{c^2(\xi^2 - 1)(1 - \eta^2)}\frac{\partial^2\phi}{\partial\varphi^2} = 0 \tag{A5}$$

provided adequate boundary conditions are given.

As posed, the problem has an analytical solution, which can be obtained by superposition of the separate effects of a net charge Q (and no external field) and the separate components of an external electric field $\boldsymbol{E}_\infty$ of arbitrary orientation (for an uncharged body). The solution to Eq. (A5) of the separate effects is summarized in Table A1, for any (ξ, η, φ) outside the ellipsoid. A parallel external field $E_{z,\infty}$ refers to a field aligned with the axis of revolution of the ellipsoid. A transverse external field refers to a field orthogonal to the axis of revolution of the ellipsoid, taken along the x direction.

On the body surface ($\xi = \xi_0$), E_ξ is the normal field E_n, and the other components are zero since the ellipsoid is conductive. Table A2 summarizes the normal fields on the ellipsoid E_n.

As an example, for a parallel field and for large ξ_0 ($\lambda \approx 1$, sphere), the maximum surface field can be obtained from the equation in Table A2: $E_n \approx 3E_{z,\infty}$, recovering the known amplification factor of 3 for a sphere.

For a transverse field, the maximum amplification now happens for $\varphi = 0$ and $\eta = 0$, and for large ξ_0, the solution for a sphere is again recovered: $E_{\max}/E_{x,\infty} \approx 3$. At the opposite limit of a slender body (ξ_0 near unity), the limit is $E_{\max}/E_{x,\infty} \approx 2$, corresponding to a cylinder in a cross-field.

For the general case of a charged ellipsoid in an external field of arbitrary orientation, the potential and the field components due to both distant fields and net charge are simply the sum of those due to each alone, Eqs. (2) and (3).

The body potential ϕ_0 only depends on the geometry and the net charge condition (C is the self-capacitance of the ellipsoid):

$$\phi_0 = C^{-1}Q = \left(\frac{1}{4\pi\varepsilon_0 c}\ell_n\sqrt{\frac{\xi_0 + 1}{\xi_0 - 1}}\right)Q \tag{A6}$$

Appendix B: Ion Flow About Charged Conductive Ellipsoid in Presence of Wind

The effect on the ion trajectories of a relative wind aligned with the axis of revolution of an ellipsoid can be evaluated analytically, provided one neglects the shielding effect of the space charge due to the ions themselves. Since the wind typically dominates over the field-induced drift, this assumption may introduce only small errors. Let U_∞ be the magnitude of the wind far from the body, and assume its direction is along z. Neglecting viscous effects and assuming subsonic flow, the flow around the body is ideal and can be derived from a harmonic potential. More useful for us is the corresponding stream function Ψ_U:

$$\Psi_U = -\frac{1}{2}U_\infty c^2(\xi^2 - 1)(1 - \eta^2) \times\left(\frac{\xi/(\xi^2 - 1) - \ell_n\sqrt{(\xi + 1)/(\xi - 1)}}{\xi_0/(\xi_0^2 - 1) - \ell_n\sqrt{(\xi_0 + 1)/(\xi_0 - 1)}} - 1\right) \tag{B1}$$

For $\xi = \xi_0$, $\Psi_U = 0$, and far from the body, $\Psi_U \to -(1/2)U_\infty c^2 R^2$, as it should. In terms of Ψ_U, the local air velocity components are given by

$$(v_\xi, v_\eta, v_\varphi) = \left(-\frac{1}{Rh_\eta}\frac{\partial\Psi_U}{\partial\eta}, \frac{1}{Rh_\xi}\frac{\partial\Psi_U}{\partial\xi}, 0\right) \tag{B2}$$

where h are the shape factors.

Table A1 Prestrike electrostatics of an ellipsoid of revolution (outside volume solution)

Potential, field	Net body charge Q	Parallel electric field $E_{z,\infty}$	Transverse electric field $E_{x,\infty}$
ϕ	$\frac{Q}{4\pi\varepsilon_0 c}\ell_n\sqrt{\frac{(\xi+1)}{(\xi-1)}}$	$-cE_{z,\infty}\eta\left(\xi-\xi_0\frac{\xi\,\ell_n\sqrt{\frac{(\xi+1)}{(\xi-1)}}-1}{\xi_0\,\ell_n\sqrt{\frac{(\xi_0+1)}{(\xi_0-1)}}-1}\right)$	$-E_{x,\infty}c\sqrt{(\xi^2-1)(1-\eta^2)}\cos\varphi\cdot\left(1-\frac{\ell_n\sqrt{\frac{(\xi+1)}{(\xi-1)}}-\frac{\xi}{(\xi^2-1)}}{\ell_n\sqrt{\frac{(\xi_0+1)}{(\xi_0-1)}}-\frac{\xi_0}{(\xi_0^2-1)}}\right)$
E_ξ	$\frac{Q/(4\pi\varepsilon_0 c^2)}{\sqrt{(\xi^2-\eta^2)(\xi^2-1)}}$	$E_{z,\infty}\eta\sqrt{\frac{(\xi^2-1)}{(\xi^2-\eta^2)}}\cdot\left(1-\frac{\xi_0}{\xi_0\,\ell_n\sqrt{\frac{(\xi_0+1)}{(\xi_0-1)}}-1}\left(\ell_n\sqrt{\frac{(\xi+1)}{(\xi-1)}}-\frac{\xi}{(\xi^2-1)}\right)\right)$	$E_{x,\infty}\xi\sqrt{\frac{(1-\eta^2)}{(\xi^2-\eta^2)}}\cos\varphi\cdot\left(1-\frac{\ell_n\sqrt{\frac{(\xi+1)}{(\xi-1)}}-\frac{(\xi-2/\xi)}{(\xi^2-1)}}{\ell_n\sqrt{\frac{(\xi_0+1)}{(\xi_0-1)}}-\frac{\xi_0}{(\xi_0^2-1)}}\right)$
E_η	0	$E_{z,\infty}\sqrt{\frac{(1-\eta^2)}{(\xi^2-\eta^2)}}\left(\xi-\xi_0\frac{\xi\,\ell_n\sqrt{\frac{(\xi+1)}{(\xi-1)}}-1}{\xi_0\,\ell_n\sqrt{\frac{(\xi_0+1)}{(\xi_0-1)}}-1}\right)$	$-E_{x,\infty}\eta\sqrt{\frac{(\xi^2-1)}{(\xi^2-\eta^2)}}\cos\varphi\cdot\left(1-\frac{\ell_n\sqrt{\frac{(\xi+1)}{(\xi-1)}}-\frac{\xi}{(\xi^2-1)}}{\ell_n\sqrt{\frac{(\xi_0+1)}{(\xi_0-1)}}-\frac{\xi_0}{(\xi_0^2-1)}}\right)$
E_φ	0	0	$-E_{x,\infty}\sin\varphi\left(1-\frac{\ell_n\sqrt{\frac{(\xi+1)}{(\xi-1)}}-\frac{\xi}{(\xi^2-1)}}{\ell_n\sqrt{\frac{(\xi_0+1)}{(\xi_0-1)}}-\frac{\xi_0}{(\xi_0^2-1)}}\right)$

Table A2 Normal field E_n on ellipsoid's surface ($\xi=\xi_0$)

Net body charge Q	Parallel electric field $E_{z,\infty}$	Transverse electric field $E_{x,\infty}$
$\frac{Q/(4\pi\varepsilon_0 c^2)}{\sqrt{(\xi_0^2-\eta^2)(\xi_0^2-1)}}$	$E_{z,\infty}\frac{\eta}{\sqrt{(\xi_0^2-\eta^2)(\xi_0^2-1)}}\frac{1}{\xi_0\,\ell_n\sqrt{\frac{(\xi_0+1)}{(\xi_0-1)}}-1}$	$-2E_{x,\infty}\sqrt{\frac{1-\eta^2}{\xi_0^2-\eta^2}}\cos\varphi\times\frac{1}{(\xi_0^2-1)\,\ell_n\sqrt{\frac{(\xi_0+1)}{(\xi_0-1)}}-\xi_0}$

After some algebra, they become

$$v_\xi=-U_\infty\sqrt{\frac{\xi^2-1}{\xi^2-\eta^2}}\eta\left(\frac{\xi/(\xi^2-1)-\ell_n\sqrt{(\xi+1)/(\xi-1)}}{\xi_0/(\xi_0^2-1)-\ell_n\sqrt{(\xi_0+1)/(\xi_0-1)}}-1\right) \tag{B3}$$

$$v_\eta=-U_\infty\sqrt{\frac{1-\eta^2}{\xi^2-\eta^2}}\xi\left(\frac{\xi/(\xi^2-1)-\ell_n\sqrt{(\xi+1)/(\xi-1)}}{\xi_0/(\xi_0^2-1)-\ell_n\sqrt{(\xi_0+1)/(\xi_0-1)}}-1\right)+\frac{U_\infty}{\xi^2-1}\sqrt{\frac{1-\eta^2}{\xi^2-\eta^2}}\frac{1}{\xi_0/(\xi_0^2-1)-\ell_n\sqrt{(\xi_0+1)/(\xi_0-1)}} \tag{B4}$$

The contribution of the electric drift, for an ion of which the mobility is μ_i and its charge is q, is

$$\boldsymbol{v}_i=\mathrm{sign}(q)\mu_i\boldsymbol{E} \tag{B5}$$

When the electric field is along z, the problem has axial symmetry about z, and a stream function Ψ then can be defined also for the contribution of the electric field:

$$\mathrm{sign}(q)\mu_i E_\xi=-\frac{1}{Rh_\eta}\frac{\partial\Psi_E}{\partial\eta} \tag{B6}$$

$$\mathrm{sign}(q)\mu_i E_\eta=\frac{1}{Rh_\xi}\frac{\partial\Psi_E}{\partial\xi} \tag{B7}$$

The function Ψ_E is constant along the field lines (lines tangent to the field). Since the field components are already known, Ψ_E can be calculated easily. We find for the part due to the charge

$$\Psi_Q=\mathrm{sign}(q)\mu_i\frac{Q_{\mathrm{ac}}}{4\pi\varepsilon_0}(1-\eta) \tag{B8}$$

and for the part due to the axial field

$$\Psi_{E_{z,\infty}}=\mathrm{sign}(q)\mu_i E_{z,\infty}c^2\frac{1-\eta^2}{2}(\xi^2-1)\times\left[1+\frac{\xi_0}{\xi_0\,\ell_n\sqrt{(\xi_0+1)/(\xi_0-1)}-1}\left(\frac{\xi}{\xi^2-1}-\ell_n\sqrt{\frac{\xi+1}{\xi-1}}\right)\right] \tag{B9}$$

The effects of charge, axial field, and wind can now be combined. We define the charge and wind parameters, respectively,

$$\bar{Q}=\frac{Q_{\mathrm{ac}}}{4\pi\varepsilon_0 c^2 E_\infty},\qquad \bar{U}=\frac{U_\infty}{\mu_i E_\infty} \tag{B10}$$

and obtain the combined nondimensional flow stream function:

$$\bar{\Psi} = -\frac{1}{2}\bar{U}(\xi^2-1)(1-\eta^2)\left[\frac{\xi/(\xi^2-1)-\ell_n\sqrt{(\xi+1)/(\xi-1)}}{\xi_0/(\xi_0^2-1)-\ell_n\sqrt{(\xi_0+1)/(\xi_0-1)}}-1\right] + \text{sign}(q)\bar{Q}(1-\eta) + \text{sign}(q)\frac{1-\eta^2}{2}(\xi^2-1) \times\left[1+\frac{\xi_0}{\xi_0\,\ell_n\sqrt{(\xi_0+1)/(\xi_0-1)}-1}\left(\frac{\xi}{\xi^2-1}-\ell_n\sqrt{\frac{\xi+1}{\xi-1}}\right)\right] \tag{B11}$$

From this combined stream function, the ion trajectories coincide with the iso-$\bar{\Psi}$ lines.

A positive ion needs to be launched from the positive end of the fuselage: $\sigma(\xi_0, \eta_0, \varphi_0) > 0$ (σ is the surface charge). From Table A2, the surface charge on the ellipsoid is given by

$$\frac{\sigma}{\varepsilon_0 E_\infty} = \frac{E_n}{E_\infty} = \frac{1}{\sqrt{(\xi_0^2-\eta^2)(\xi_0^2-1)}}\left(\frac{\eta}{\xi_0\,\ell_n\sqrt{(\xi_0+1)/(\xi_0-1)}-1}+\bar{Q}\right) \tag{B12}$$

So, ion emission needs to start from

$$\eta_0 > -\bar{Q}\left(\xi_0\,\ell_n\sqrt{\frac{\xi_0+1}{\xi_0-1}}-1\right) \tag{B13}$$

The trajectory the positive ion will follow upon emission is given by the implicit equation

$$\bar{\Psi}_0 = \bar{\Psi}(\xi_0, \eta_0, \varphi_0) = A(\xi; \xi_0, \bar{U})(1-\eta^2) + \bar{Q}(1-\eta) \tag{B14}$$

with

$$A(\xi; \xi_0, \bar{U}) = B(\xi; \xi_0, \bar{U}) + C(\xi; \xi_0) \tag{B15}$$

$$B(\xi;\xi_0,\bar{U}) = -\frac{1}{2}\bar{U}(\xi^2-1)\left(\frac{\xi/(\xi^2-1)-\ell_n\sqrt{(\xi+1)/(\xi-1)}}{\xi_0/(\xi_0^2-1)-\ell_n\sqrt{(\xi_0+1)/(\xi_0-1)}}-1\right) \tag{B16}$$

$$C(\xi;\xi_0) = \frac{1}{2}(\xi^2-1) \times\left[1+\frac{\xi_0}{\xi_0\,\ell_n\sqrt{(\xi_0+1)/(\xi_0-1)}-1}\left(\frac{\xi}{\xi^2-1}-\ell_n\sqrt{\frac{\xi+1}{\xi-1}}\right)\right] \tag{B17}$$

which can be rearranged to obtain η explicitly from ξ:

$$\eta(\xi;\xi_0,\bar{U},\bar{Q},\Psi_0) = \frac{-\bar{Q}\pm\sqrt{\bar{Q}^2-4A(\Psi_0-\bar{Q}-A)}}{2A} \tag{B18}$$

For an example, let us consider an ellipsoid with aspect ratio $\lambda = 7$ and $c = 17.5$ m, representative of the Falcon geometry used in

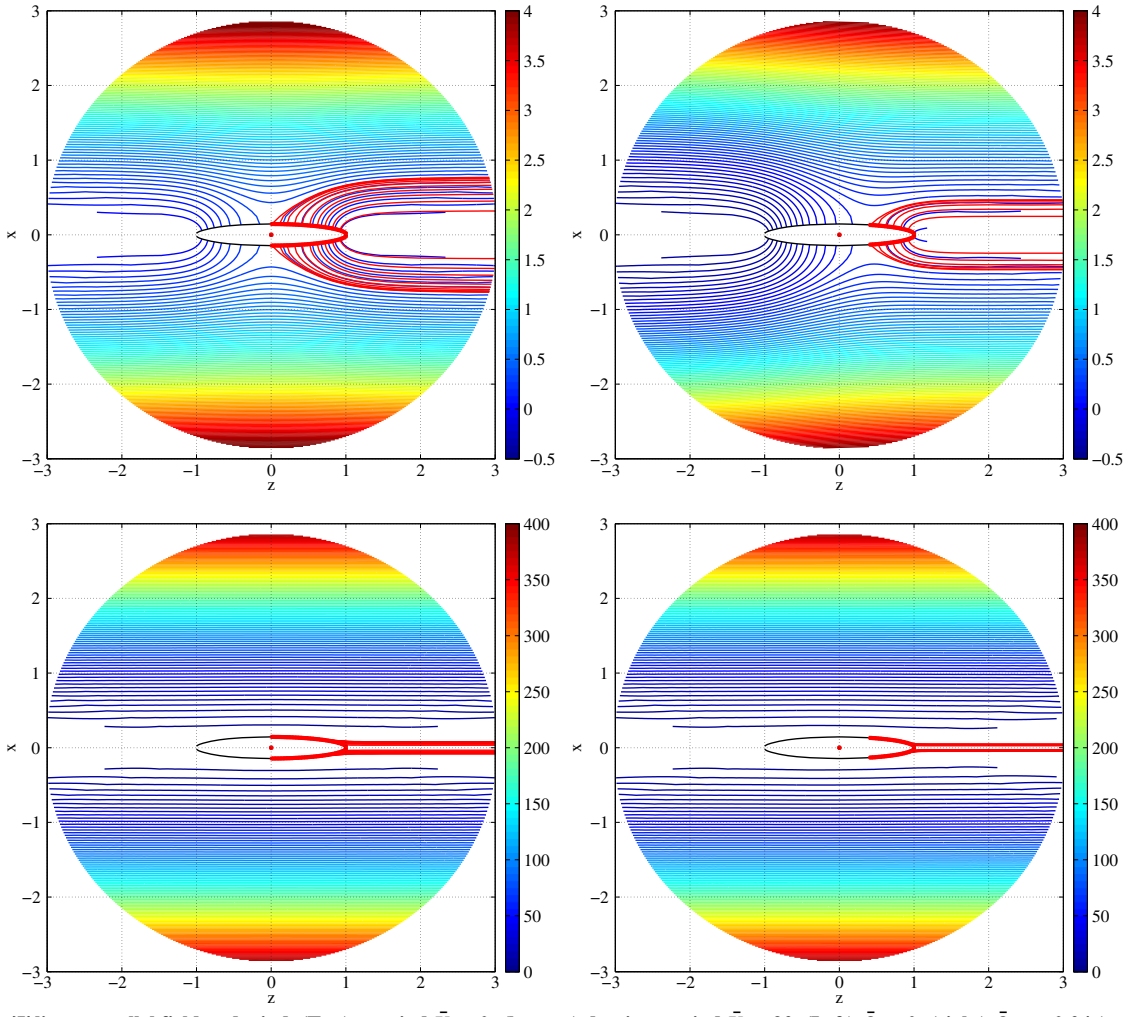

Fig. B1 Iso-Ψ lines, parallel field and wind. (Top) no wind $\bar{U} = 0$; (bottom) dominant wind $\bar{U} = 92$. (Left) $\bar{Q} = 0$; (right) $\bar{Q} = -0.24$ (optimum). The trajectories followed by positive ions, launched from select points on the surface, are marked in red.

Sec. III. In the absence of a net body charge, the maximum field on its surface is $E_{\max} \approx 30E_\infty$ [Eq. (10)]. Taking the positive breakdown threshold as the stability field of the positive corona $E_{\text{cr}}^+ \approx 450$ kV/m, an external field of the order of $E_\infty \approx 15$ kV/m will suffice to initiate a positive leader. By using the charge control strategy, the ellipsoid can overcome this limit and fly through regions for which the external field is up to 50% higher. For example, for an external field of $E_\infty = 19.5$ kV/m, the aircraft can still fly safely if its charge is given by Eq. (9), $Q_{\text{opt}} = Q_{\text{opt}}/4\pi\varepsilon_0 c^2 E_\infty = -0.24$, or recovering units $Q_{\text{opt}} = -160\ \mu$C. For this charge condition, the safety margins for the positive and negative discharges are equal: $E_{\text{cr}}^+ - E_{\max} = E_{\text{cr}}^- - (-E_{\min}) \approx 5.8E_\infty \sim 115$ kV/m, and leaders will not be incepted.

In this situation, the terminal electric drift, far from the fuselage, is $\mu_i E_\infty = 2.73$ m/s ($\mu_i = 1.4$ cm^2/V/s at atmospheric conditions). This speed is much lower than the magnitude of the wind $U_\infty \approx 250$ m/s, so the wind will dominate the ion trajectories: $\bar{U} \approx 92$.

Figure B1 shows the iso-Ψ lines in this situation, which coincide with the trajectories positive ions would follow. The surface of the ellipsoid that is positively charged is marked in red (region from which positive ions can be launched). The surface of the ellipsoid that is negatively charged is marked in black. In the absence of a wind, the ion trajectories coincide with the electric field lines. It can be appreciated that, as positive charge is emitted from the body and the fuselage is biased toward more negative values, the region from which positive ions can be emitted becomes smaller.

For any other case, with no axial symmetry, the ion trajectories need to be integrated numerically from the velocity vector field,

$$\frac{d}{dt}(\xi, \eta, \varphi) = \left(\frac{v_\xi}{h_\xi}, \frac{v_\eta}{h_\eta}, \frac{v_\varphi}{h_\varphi}\right) \tag{B19}$$

with initial conditions (ξ_0, η_0, φ_0) that satisfy $(\sigma/\varepsilon_0 E_\infty) > 0$ (positive ions).

For an example, in what follows, we evaluate the ion trajectories from an ellipsoid in parallel wind and transverse field. Note that this is a very conservative case since, for $Q_{\text{ac}} = 0$, the maximum field on the ellipsoid is only $E_{\max} \approx 2.1E_\infty$ and so a very large external field, $E_\infty \approx 215$ kV/m, will be required to initiate a positive leader. When using charge control, this field can further be increased; e.g., for an external field of 250 kV/m, the optimum charge condition [evaluated numerically from Eq. (8)] is $Q_{\text{opt}} = -0.058$. In this case, the wind parameter becomes $\bar{U} \approx 7$.

The ion trajectories from the positive end are shown in Fig. B2, for the initial uncharged condition and the moment when the optimum level is reached. The surface of the ellipsoid that is positively charged is marked in red (region from which positive ions can be launched). The surface of the ellipsoid that is negatively charged is marked in black. As before, the region from where positive ions can be launched is reduced as the fuselage is charged negatively, so ion emitters should be placed at the regions where the radius of curvature is smaller. In this case, both the contribution of the wind and the electric drift are comparable, and both contribute to the evacuation of the ions away from the surface.

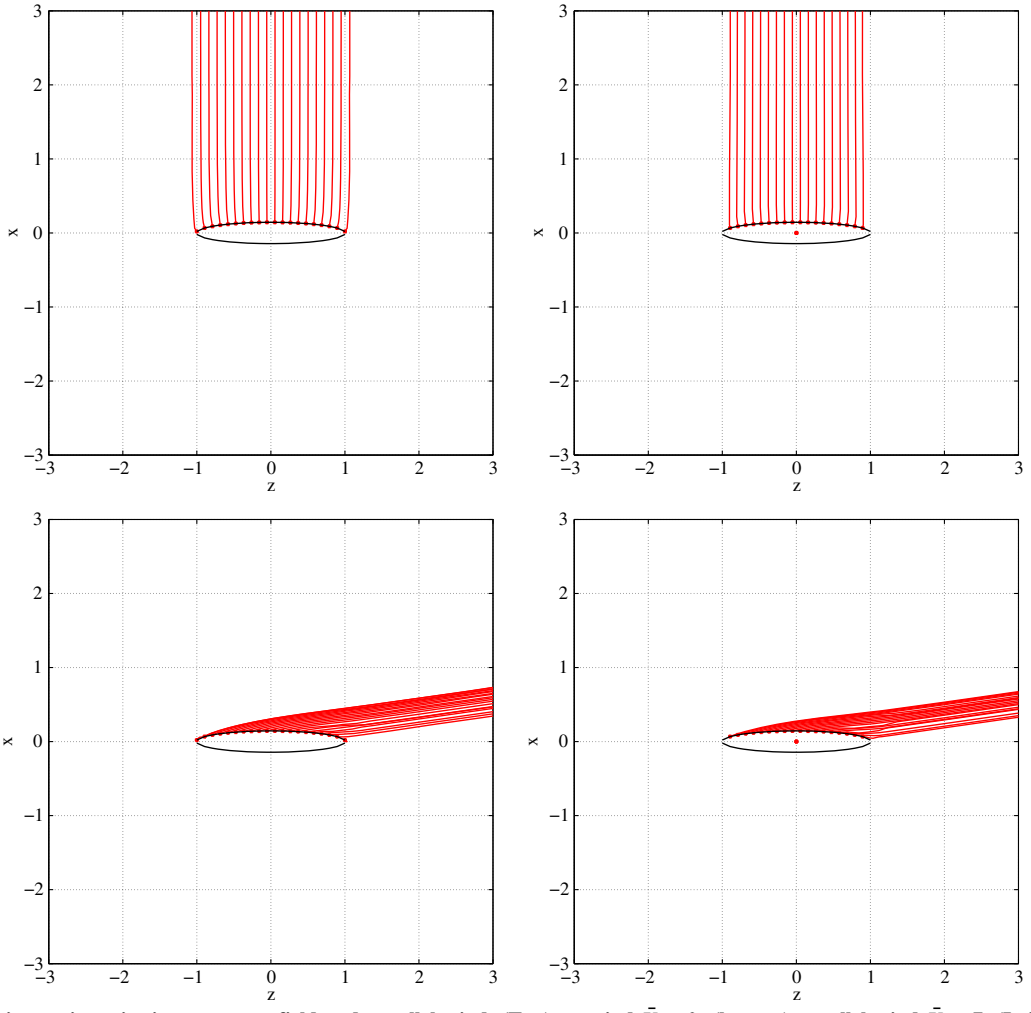

Fig. B2 Positive ion trajectories in transverse field and parallel wind. (Top) no wind $\bar{U} = 0$; (bottom) parallel wind $\bar{U} = 7$. (Left) $\bar{Q} = 0$; (right) $\bar{Q} = -0.058$ (optimum). The trajectories followed by positive ions, launched from select points on the surface, are marked in red.

Acknowledgments

This work was supported by The Boeing Company through the Strategic Universities for Boeing Research and Technology Program. N. C. Nguyen and J. Peraire acknowledge partial support from the Air Force Office of Scientific Research through grant number FA9550-16-1-0214. The authors would like to thank Xevi Roca (Barcelona Supercomputing Center) for preparing the geometry and meshing of the Falcon aircraft used in the numerical simulations.

References

[1] Fisher, F. A., Plumer, J. A., and Perala, R. A., *Lightning Protection of Aircraft*, 2nd ed., Lightning Technologies Inc., Pittsfield, MA, 2004, pp. 37–56.

[2] Lalande, P., Bondiou-Clergerie, A., and Laroche, P., "Analysis of Available In-Flight Measurements of Lightning Strikes to Aircraft," *Proceedings of the 1999 International Conference on Lightning and Static Electricity (ICOLSE)*, Soc. of Automotive Engineers International Paper 1999-01-2397, 1999. doi:10.4271/1999-01-2397

[3] Moreau, J. P., Alliot, J. C., and Mazur, V., "Aircraft Lightning Initiation and Interception from In Situ Electric Measurements and Fast Video Observations," *Journal of Geophysical Research*, Vol. 95, No. 15, 1992, pp. 903–912.

[4] Larsson, A., "The Interaction Between a Lightning Flash and an Aircraft in Flight," *Comptes Rendus Physique*, Vol. 3, No. 10, 2002, pp. 1423–1444. doi:10.1016/S1631-0705(02)01410-X

[5] Rakov, V. A., and Uman, M. A., *Lightning Physics and Effects*, Cambridge Univ. Press, Cambridge, England, U.K., 2003, pp. 346–373.

[6] Laroche, P., Blanchet, P., Delannoy, A., and Issac, F., "Experimental Studies of Lightning Strikes to Aircraft," *Journal AerospaceLab*, Vol. 5, No. 1, 2012, Paper AL05-06.

[7] Fitzgerald, D. R., "Probable Aircraft Triggering of Lightning in Certain Thunderstorms," *Monthly Weather Review*, Vol. 95, No. 12, 1967, pp. 835–842. doi:10.1175/1520-0493(1967)095<0835:PATOLI>2.3.CO;2

[8] Petterson, B. J., and Wood, W. R., "Measurements of Lightning Strikes to Aircraft," Rept. SC-M-67-549, Sandia Laboratories, Albuquerque, NM, 1968.

[9] Fisher, B. D., "Lightning Swept-Stroke Attachment Patterns and Flight Conditions for Storm Hazards '81," NASA TM 86279, 1984.

[10] Fisher, B. D., and Plumer, J. A., "Lightning Attachment Patterns and Flight Conditions Experienced by the NASA F-106B Airplane from 1980 to 1983," *AIAA 22nd Aerospace Sciences Meeting*, AIAA Paper 1984-0466, 1984.

[11] Trost, T. F., and Zaepfel, K. P., "Broadband Electromagnetic Sensors for Lightning Research," NASA Langley Research Center Rept. CP-2128, FAA-RD-8-30, 1980, pp. 131–152.

[12] Pitts, F. L., and Thomas, M. E., "1980 Direct Strike Lightning Data," NASA Langley Research Center TM 81946, 1981.

[13] Pitts, F. L., "Electromagnetic Measurement of Lightning Strikes to Aircraft," *Journal of Aircraft*, Vol. 19, No. 3, 1982, pp. 246–250. doi:10.2514/3.57383

[14] Pitts, F. L., and Thomas, M. E., "1981 Direct Strike Lightning Data," NASA Langley Research Center TM 83273, 1982.

[15] Thomas, M. E., "Direct Strike Lightning Measurement System," *AIAA/SETP/SFTE/SAE/ITEA/IEEE 1st Flight Testing Conference*, AIAA Paper 1981-2513, 1981.

[16] Thomas, M. E., and Pitts, F. L., "1982 Direct Strike Lightning Data," NASA TM 84626, 1983.

[17] Lee, L. D., Finelli, G. B., Thomas, M. E., and Pitts, F. L., "Statistical Analysis of Direct-Strike Lightning Data," NASA Langley Research Center Rept. TP-2252, 1984, pp. 1–27.

[18] Mazur, V., Fisher, B. D., and Gerlach, J. C., "Lightning Strikes to an Airplane in a Thunderstorm," *Journal of Aircraft*, Vol. 21, No. 8, 1984, pp. 607–611. doi:10.2514/3.45030

[19] Mazur, V., Fisher, B. D., and Gerlach, J. C., "Lightning Strikes to a NASA Airplane Penetrating Thunderstorms at Low Altitudes," *Journal of Aircraft*, Vol. 23, No. 6, 1986, pp. 499–505. doi:10.2514/3.45335

[20] Mazur, V., and Fisher, B. D., "Cloud-to-Ground Strikes to the NASA F-106 Airplane," *Journal of Aircraft*, Vol. 27, No. 5, 1990, pp. 466–468. doi:10.2514/3.25302

[21] Zaepfel, K. P., Fisher, B. D., and Ott, M. S., "Direct-Strike Lightning Photographs, Swept-Flash Attachment Patterns, and Flight Conditions for Storm Hazards '82," NASA TM 86347, 1985.

[22] Rustan, P. L., "The Lightning Threat to Aerospace Vehicles," *Journal of Aircraft*, Vol. 23, No. 1, 1986, pp. 62–67. doi:10.2514/3.45267

[23] Reazer, J. S., Serrano, A. V., Walko, L. C., and Burket, H. D., "Analysis of Correlated Electromagnetic Fields and Current Pulses During Airborne Lightning Attachments," *Electromagnetics*, Vol. 7, Nos. 3–4, 1987, pp. 509–539. doi:10.1080/02726348708908196

[24] Mazur, V., "A Physical Model of Lightning Initiation on Aircraft in Thunderstorms," *Journal of Geophysical Research*, Vol. 94, No. D3, 1989, pp. 3326–3340. doi:10.1029/JD094iD03p03326

[25] Mazur, V., and Moreau, J. P., "Aircraft-Triggered Lightning: Processes Following Strike Initiation That Affect Aircraft," *Journal of Aircraft*, Vol. 29, No. 4, 1992, pp. 575–580. doi:10.2514/3.46204

[26] Saba, M., Schumann, C., Warner, T. A., Ferro, M. A. S., de Paiva, A. R., Helsdon, J., Jr., and Orville, R. E., "Upward lightning Flashes Characteristics from High-Speed Videos," *Journal of Geophysical Research: Atmospheres*, Vol. 121, No. 14, 2016, pp. 849–8505. doi:10.1002/2016JD025137

[27] Mazur, V., "Lightning Initiation on Aircraft in Thunderstorms," *AIAA 26th Aerospace Sciences Meeting*, AIAA Paper 1988-0391, 1988.

[28] Mazur, V., "Triggered Lightning Strikes to Aircraft and Natural Intracloud Discharges," *Journal of Geophysical Research*, Vol. 94, No. D3, 1989, pp. 3311–3325. doi:10.1029/JD094iD03p03311

[29] Plumer, J. A., Rasch, N. O., and Glynn, M. S., "Recent Data from the Airlines Lightning Strike Reporting Project," *Journal of Aircraft*, Vol. 22, No. 5, 1985, pp. 429–433. doi:10.2514/3.45142

[30] Montanya, J., van der Velde, O., and Williams, E. R., "The Start of Lightning: Evidence of Bidirectional Lightning Initiation," *Scientific Reports*, Vol. 5, No. 1, 2015, Paper 15180. doi:10.1038/srep15180

[31] Tran, M. D., and Rakov, V. A., "Initiation and Propagation of Cloud-to-Ground Lightning Observed with a High-Speed Video Camera," *Scientific Reports*, Vol. 6, No. 1, 2016, Paper 39521. doi:10.1038/srep39521

[32] Perala, R. A., and Rudolph, T. H., "Triggering of Lightning by Aerospace Vehicles," *AIAA 26th Aerospace Sciences Meeting*, AIAA Paper 1988-0393, 1988.

[33] Mazur, V., "Lightning Threat to Aircraft: Do We Know All We Need to Know?" *Journal of Aircraft*, Vol. 30, No. 1, 1993, pp. 156–159. doi:10.2514/3.46330

[34] Pitts, F. L., Perala, R. A., Rudolph, T. H., and Lee, L. D., "New Results for Quantification of Lightning/Aircraft Electrodynamics," *Electromagnetics*, Vol. 7, Nos. 3–4, 1987, pp. 451–485. doi:10.1080/02726348708908194

[35] Lalande, P., Bondiou-Clergerie, A., and Laroche, P., "Computations of the Initial Discharge Initiation Zones on Aircraft or Helicopter," *Proceedings of the 1999 International Conference on Lightning and Static Electricity (ICOLSE)*, Soc. of Automotive Engineers International Paper 1999-01-2371, 1999. doi:10.4271/1999-01-2371

[36] Zaglauer, H., and Wulbrand, W., "A Simplified Model for the Determination of Initial Attachment Zones via Electric Field Modeling - Parameter Studies and Comparisons," *Proceedings of the 1999 International Conference on Lightning and Static Electricity (ICOLSE)*, Soc. of Automotive Engineers International Paper 1999-01-2375, 1999. doi:10.4271/1999-01-2375

[37] Lalande, P., and Delannoy, A., "Numerical Methods for Zoning Computation," *Journal AerospaceLab*, Vol. 5, No. 1, 2012, pp. AL05–AL08.

[38] Krozel, J., Deierling, W., Sharman, R. D., and Williams, J. K., "Detecting Convective Induced Turbulence via Total Lightning Sensing," *AIAA Guidance, Navigation, and Control Conference*, AIAA Paper 2015-1548, 2015.

[39] Corn, P. B., "Aircraft and Environmental Factors Influencing Lightning Strike," *AIAA 19th Aerospace Sciences Meeting*, AIAA Paper 1981-0084, 1981.

[40] Vonnegut, B., and Little, A. D., "Electrical Behavior of an Airplane in a Thunderstorm," Tech. Rept. FAA–ADS–36, Federal Aviation Agency, 1965.

[41] Jones, J. J., "Electric Charge Acquired by Airplanes Penetrating Thunderstorms," *Journal of Geophysical Research*, Vol. 95, No. D10,

1990, pp. 16589–16600.
doi:10.1029/JD095iD10p16589

[42] Nguyen, N. C., Peraire, J., and Cockburn, B., "An Implicit High-Order Hybridizable Discontinuous Galerkin Method for Nonlinear Convection Diffusion Equations," *Journal of Computational Physics*, Vol. 228, No. 23, Dec. 2009, pp. 8841–8855.
doi:10.1016/j.jcp.2009.08.030

[43] Nguyen, N. C., Peraire, J., and Cockburn, B., "An Implicit High-Order Hybridizable Discontinuous Galerkin Method for the Incompressible Navier-Stokes Equations," *Journal of Computational Physics*, Vol. 230, No. 4, Feb. 2011, pp. 1147–1170.
doi:10.1016/j.jcp.2010.10.032

[44] Nguyen, N. C., and Peraire, J., "Hybridizable Discontinuous Galerkin Methods for Partial Differential Equations in Continuum Mechanics," *Journal of Computational Physics*, Vol. 231, No. 18, 2012, pp. 5955–5988.
doi:10.1016/j.jcp.2012.02.033

[45] Gallimberti, I., "The Mechanism of the Long Spark Formation," *Journal de Physique Colloques*, Vol. 40, No. C7, 1979, pp. 193–250.

[46] Les Renardieres Group, "Research on Long Gap Discharges at Les Renardieres," *Electra*, Vol. 23, 1973, pp. 53–157.

[47] Castellani, A., Bondiou-Clergerie, A., Lalande, P., Bonamy, A., and Gallimberti, I., "Laboratory Study of the Bi-Leader Process from an Electrically Floating Conductor. Part 2: Bi-Leader Properties," *IEE Proceedings: Science, Measurement and Technology*, Vol. 145, No. 5, 1998, pp. 193–199.
doi:10.1049/ip-smt:19982011

[48] Lalande, P., Bondiou-Clergerie, A., Bacchiega, G., and Gallimberti, I., "Observations and Modeling of Lightning Leaders," *Comptes Rendus Physique*, Vol. 3, No. 10, 2002, pp. 1375–1392.
doi:10.1016/S1631-0705(02)01413-5

[49] Gallimberti, I., Bacchiega, G., Bondiou-Clergerie, A., and Lalande, P., "Fundamental Processes in Long Air Gap Discharges," *Comptes Rendus Physique*, Vol. 3, No. 10, 2002, pp. 1335–1359.
doi:10.1016/S1631-0705(02)01414-7

[50] Cooray, V., *An Introduction to Lightning*, Springer–Verlag, Berlin, 2014, pp. 7–27.

[51] Arevalo, L., Cooray, V., and Montano, R., "Numerical Simulation of Long Laboratory Sparks Generated by Positive Switching Impulses," *Journal of Electrostatics*, Vol. 67, Nos. 2–3, 2009, pp. 228–234.
doi:10.1016/j.elstat.2008.12.022

[52] Arevalo, L., Cooray, V., and Wu, D., "Laboratory Long Gaps Simulation Considering a Variable Corona Region," *Proceedings of the 30th International Conference on Lightning Protection*, IEEE Paper 1159, Piscataway, NJ, 2010.
doi:10.1109/ICLP.2010.7845875

[53] Arevalo, L., Cooray, V., Wu, D., and Jacobson, B., "A New Static Calculation of the Streamer Region for Long Spark Gaps," *Journal of Electrostatics*, Vol. 70, No. 1, 2012, pp. 15–19.
doi:10.1016/j.elstat.2011.07.013

[54] Becerra, M., and Cooray, V., "A Simplified Physical Model to Determine the Lightning Upward Connecting Leader Inception," *IEEE Transactions on Power Delivery*, Vol. 21, No. 2, 2006, pp. 897–908.
doi:10.1109/TPWRD.2005.859290

[55] Niemeyer, L., *Gaseous Dielectrics IV. Section on Leader Breakdown in Compressed SF_6 Recent Concepts and Understanding*, Plenum, New York, 1991, Chap. 2, pp. 49–60.

[56] Montanya, J., van der Velde, O., and Williams, E. R., "Lightning Discharges Produced by Wind Turbines," *Journal of Geophysical Research: Atmospheres*, Vol. 119, No. 3, 2014, pp. 1455–1462.
doi:10.1002/2013JD020225

[57] Becerra, M., Cooray, V., Soula, S., and Chauzy, S., "Effect of the Space Charge Layer Created by Corona at Ground Level on the Inception of Upward Lightning Leaders from Tall Towers," *Journal of Geophysical Research*, Vol. 112, No. D12, 2007, Paper D12205.
doi:10.1029/2006JD008308

[58] Becerra, M., and Cooray, V., "A Self-Consistent Upward Leader Propagation Model," *Journal of Physics D: Applied Physics*, Vol. 39, No. 16, 2006, pp. 3708–3715.
doi:10.1088/0022-3727/39/16/028

[59] Goelian, N., Lalande, P., Bondiou-Clergerie, A., and Bacchiega, G., "A Simplified Model for the Simulation of Positive-Spark Development in Long Air Gaps," *Journal of Physics D: Applied Physics*, Vol. 30, No. 17, 1997, pp. 2441–2452.
doi:10.1088/0022-3727/30/17/010

[60] Becerra, M., Cooray, V., and Roman, F., "Lightning Striking Distance of Complex Structures," *IET Generation, Transmission and Distribution*, Vol. 2, No. 1, 2008, pp. 131–138.
doi:10.1049/iet-gtd:20070099

[61] Lowke, J. J., and Alessandro, F. D., "Onset Corona Fields and Electrical Breakdown Criteria," *Journal of Physics D: Applied Physics*, Vol. 36, No. 21, 2003, pp. 2673–2682.
doi:10.1088/0022-3727/36/21/013

[62] Guerra-Garcia, C., Nguyen, N. C., Peraire, J., and Martinez-Sanchez, M., "Influence of Net Charge on the Probability of Lightning Initiation from Aircraft," *Proceedings of the 2017 International Conference on Lightning and Static Electricity (ICOLSE)*, Inst. of Engineering and Technology (IET), 2017, Paper 1019.

[63] Martinez-Sanchez, M., Guerra-Garcia, C., Nguyen, N. C., Peraire, J., and Mouratidis, T., Massachusetts Inst. of Technology, Cambridge, MA, U.S. Patent Application for "Charge Control System to Reduce Risk of an Aircraft-Initiated Lightning Strike," Docket No. 18552.123193, filed 14 April 2017.

[64] Winn, W. P., "Aircraft Measurement of Electric Field: Self-Calibration," *Journal of Geophysical Research*, Vol. 98, No. D4, 1993, pp. 7351–7365.
doi:10.1029/93JD00165

[65] Mach, D. M., and Koshak, W. J., "General Matrix Inversion Technique for the Calibration of Electric Field Sensor Arrays on Aircraft Platforms," *Journal of Atmospheric and Oceanic Technology*, Vol. 24, No. 9, 2007, pp. 1576–1587.
doi:10.1175/JTECH2080.1

[66] Anderson, R. V., and Bailey, J. C., "Vector Electric Fields Measured in a Lightning Environment," Memorandum 5899, Naval Research Lab., 1987.

[67] Koshak, W. J., "Retrieving Storm Electric Fields from Aircraft Field Mill Data. Part I: Theory," *Journal of Atmospheric and Oceanic Technology*, Vol. 23, No. 10, 2006, pp. 1289–1302.
doi:10.1175/JTECH1917.1

[68] Parker, L. W., and Kasemir, H. W., "Airborne Warning Systems for Natural and Aircraft-Initiated Lightning," *IEEE Transactions of Electromagnetic Compatibility*, Vol. EMC-24, No. 2, 1982, pp. 137–158.
doi:10.1109/TEMC.1982.304009

[69] Anway, C. E., Boeing, Chicago, IL, U.S. Patent Application for "Electric Field Whistle," Docket No. 7944361B2, filed 17 May 2011.

[70] Mier-Hicks, F., and Lozano, P. C., "Spacecraft-Charging Characteristics Induced by the Operation of Electrospray Thrusters," *Journal of Propulsion and Power*, Vol. 33, No. 2, 2017, pp. 456–467.
doi:10.2514/1.B36292

[71] Vonnegut, B., Moore, B. C., and Mallahan, F. J., "Adjustable Potential-Gradient-Measuring Apparatus for Airplane Use," *Journal of Geophysical Research*, Vol. 66, No. 8, 1961, pp. 2393–2397.
doi:10.1029/JZ066i008p02393

C. Wen
Associate Editor